Chapter 19
Meteorological Radar

R. Jeffrey Keeler and Robert J. Serafin

*National Center for Atmospheric Research**

19.1 INTRODUCTION

Standard operational meteorological doppler radars have become familiar observational tools to radar engineers as well as the general public since their introduction by the United States National Weather Service (NWS) in the 1950s and are widely used by weather forecasters in the public and private sectors. Major technical improvements were introduced in the 1990s when the NWS, the Federal Aviation Agency (FAA), and the U.S. Air Force joined together to install the next generation national network of WSR-88D doppler radars (commonly called Nexrad radars). Also in the 1990s the FAA installed the Terminal Doppler Weather Radar (TDWR) system at major airports in the U.S. The federal agencies have subsequently implemented many technical upgrades to the Nexrad and TDWR networks to improve their performance for public warnings and aviation safety.[1,2] In contrast to the WSR-57 and WSR-74C radars they replaced, the WSR-88D systems provide quantitative and automated real-time information on storms, precipitation, hurricanes, tornadoes, and a host of other important weather phenomena with higher spatial and temporal resolution than ever before.[3,4] In the aviation community, TDWR radars provide crucial information for providing safe departures and landings at the major airports by detecting hazardous wind shear events such as microbursts, strong gust fronts, and other performance reducing wind hazards.[5,6,7]

Various other types of meteorological radars exist. The Nexrad long-range weather surveillance radars are frequently supplemented by (typically) smaller medium-range weather radars operated by TV stations for local observations.[8] In addition to the familiar commercial airborne weather avoidance and observation radars, airborne hurricane monitoring provides detailed forecasts and warnings for approaching coastal hurricanes.[9] And vertical pointing wind profiling fixed-beam systems are routinely used to obtain continuous profiles of horizontal winds[10] whereas spaced-based meteorological radars are measuring widespread equatorial precipitation fields and cloud properties.[11] Meteorological research results are regularly transferred to the operational weather radar community for achieving higher space and time resolution, for improved data quality, and for the production of new weather radar products all of which have led to dramatic improvements in weather forecasting. Doppler weather radars measure detailed vector wind fields as well as precipitation fields. Small, highly mobile research radars provide many of the same capabilities as the fixed radars.[12] Dual polarization techniques[13,14] are used for improved quantitative

* The National Center for Atmospheric Research is sponsored by the National Science Foundation.

precipitation measurement, for detecting hail,[15] and for discriminating ice particles (snow) from water (rain).[16] Furthermore, ground-based research radars can now measure atmospheric moisture in the surface boundary layer.[17] Airborne research radars provide many of these same capabilities with increased coverage and greater mobility.[18] This variety of applications in both research and operations illustrates the vitality of meteorological radar technology and its evolution.

This chapter is intended to introduce the reader to meteorological radar, particularly those system characteristics that are unique to meteorological applications. In this regard, it should be noted that most meteorological radars appear similar to radars used for other purposes. Pulsed doppler systems are far more prevalent than CW radars. Primarily, center-fed parabolic dish antennas with focal-point feed and low-noise solid-state digital receivers are used. Magnetrons, klystrons, traveling-wave tubes, and other forms of transmitter forms are routinely used.

The distinguishing factor between meteorological radar and other kinds of aviation or military radars lies in the nature of weather targets, the resulting characteristics of the radar signal, and the means by which these weather echoes are processed to suppress artifacts and generate only the significant and essential weather information. Important meteorological targets occupy a wide range of scattering echo intensities (−20 to 70 dBZ) that are distributed in space from short range (< 1 km) to long range (> 200 km), close to the surface (100 m) to the top of the atmosphere where weather is important (20 km), and typically occupy a large fraction of the several millions of spatial resolution cells observed by the radar. Moreover, it is necessary to make quantitative measurements of the received signal characteristics in each of these cells, or "weather targets," to estimate such parameters as precipitation rate, precipitation type, air motion, turbulence, and wind shear.[19] In addition, because a high percentage of radar resolution cells contain useful information, meteorological radars require fast digital signal processors, effective means for suppressing artifacts caused by the data density, high data-rate recording systems, and informative displays of this information. Thus, whereas many non-weather radar applications call for detection, tracking, and detailed characterization of relatively fewer number of desired targets in a field of widespread weather, ground, sea, decoy, and bird clutter, the meteorological radars focus on making accurate estimates of the nature of the "weather clutter" itself. Both aviation/military and weather radars require heavy processing activity, but the volume of data for assimilation, recording, and display of weather radars is often much larger since different essential information must be extracted for a large number of anticipated users when measuring widespread weather systems.

The discussion herein refers to a number of useful texts and references for the reader. However, the classic *Radar Observation of the Atmosphere* by Lou Battan[20] deserves special mention for its clarity and completeness and remains a standard for courses in radar meteorology. The *Battan Memorial and 40th Anniversary Radar Meteorology Conference* produced a collection of review papers, *Radar in Meteorology,*[21] covering the first four decades of radar meteorology from the historical, technological, scientific, and operational perspectives. Bean et al.[22] in Skolnik's first *Radar Handbook* addressed the problem of weather effects on radar. Doviak and Zrnić[23] place special emphasis on doppler aspects of meteorological radar, whereas Bringi and Chandra[24] emphasize all aspects of polarimetric radars and Lhermitte[25] focuses on millimeter wave (cloud) radars. Rinehart's *Radar for Meteorologists*[26] gives a broad and easily comprehendible overview of all aspects of weather radar. The IEEE Geoscience and Electronics *Special Issue on Radar Meteorology,*[27] Atlas's *Radar in Meteorology,*[21] Wakimoto and Srivastiva's *Radar and Atmospheric Science: A Collection of Essays in Honor of David Atlas,*[28] and

Meischner's *Weather Radar*[29] provide an evolving perspective on many aspects of meteorological radars by technological and scientific leaders. Finally, perhaps the broadest and most complete set of references on progress in the field can be found in the series of *Proceedings and Preprints of the (International) Conferences on Radar Meteorology*[30] sponsored by the American Meteorological Society (AMS). These documents can be found in many technical libraries and also can be obtained online. In addition, the *Proceedings of the European Conferences on Radar Meteorology*[31] provides excellent reference material.

19.2 THE RADAR EQUATION FOR METEOROLOGICAL TARGETS

The received power P_r from a radar point target can be derived from any of a variety of expressions that are applicable to radar in general.[23,26,32] For a single point target, a simple form that is readily derived is

$$P_r = \frac{\beta\sigma}{r^4} \tag{19.1}$$

where β is a constant dependent upon radar system parameters (transmitted power P_t, antenna system gain G, and wavelength λ), r is the range to the point target, and σ is the radar cross section (RCS).*

It is in the calculation of σ for distributed meteorological targets that the radar equation differs from that for point targets. For distributed targets like rainfall the RCS may be written

$$\sigma = \eta V \tag{19.2}$$

where η is the radar reflectivity in units of cross-sectional area per unit volume and V is the volume sampled by the radar. η can itself be written as

$$\eta = \sum_{i=1}^{N} \sigma_i \tag{19.3}$$

where N is the number of scatterers per unit volume and σ_i is the backscattering cross section of the ith point scatterer. In general, the meteorological scatterers can take on a variety of forms, which include water droplets, ice crystals, hail, snow, and mixtures of the above.

Mie[33] developed a general theory for the energy backscattered by an optical plane wave impinging on conducting spheres in colloidal suspension. The same theory applies to spherical raindrops falling through the atmosphere for which the backscattered energy is a function of the wavelength (λ) of the incident energy and the radius (a) and complex index of refraction (m) of the particle. The ratio $2\pi a/\lambda$ determines the dominant scattering properties of the particle. Spherical water droplets in air that are large relative to the wavelength scatter in the so called optical region; droplets on the order of the same size as the wavelength scatter in the so called resonant scattering region; and droplets small relative to the wavelength scatter in the so-called Rayleigh region.

* By convention in this chapter, we shall use r for range and R for rainfall rate.

When the ratio $2\pi a/\lambda < 1$, the Rayleigh approximation[20] may be applied, and σ_i becomes

$$\sigma_i = \frac{\pi^5}{\lambda^4} |K|^2 D_i^6 \tag{19.4}$$

where D_i is the diameter of the ith drop and

$$|K|^2 = \left| \frac{m^2 - 1}{m^2 + 2} \right|^2 \tag{19.5}$$

where m is the complex index of refraction. At temperatures between 0 and 20°C and centimeter wavelengths, $|K|^2 \approx 0.93$ for the water phase and $|K|^2 \approx 0.197$ for the ice phase.

Equation 19.3 can now be written as

$$\eta = \frac{\pi^5}{\lambda^4} |K|^2 \sum_{i=1}^{N} D_i^6 \tag{19.6}$$

and we define the radar reflectivity factor Z as

$$Z = \sum_{i=1}^{N} D_i^6 \tag{19.7}$$

In radar meteorology, it is common to use the dimensions of millimeters for drop diameter D_i and to consider the summation to take place over a unit volume of size 1 m^3 to yield a volume density expression. Therefore, the conventional unit of Z is in mm^6/m^3. For ice particles, D_i is sometimes expressed as the diameter of the water droplet that would result if the ice particle were to melt completely. However, the radar scattering process for the many shapes and temperatures of ice particles is extremely complicated and a definitive generalized expression cannot be given.

It is often convenient to treat the drop or particle size distribution as a continuous function with a number density $N(D)$, where $N(D)$ is the number of drops per unit volume having diameters between D and $D + dD$. In this case, Z is given by the sixth moment of the particle size distribution,

$$Z = \int_0^\infty n(D) D^6 dD \tag{19.8}$$

If the radar beam is filled with scatterers, the sample volume of V is given[10] approximately by

$$V \approx \frac{\pi \theta \phi r^2 c \tau}{8} \tag{19.9}$$

where θ and ϕ are the azimuth and elevation beamwidths, c is the velocity of light, and τ is the radar pulse width. Substituting Eqs. 19.3 and 19.9 into Eq. 19.2, we see that the RCS for the distributed weather scatterer is directly proportional to the pulse volume as determined by the pulse length and antenna beam at the target range.

Then, combining Eqs. 19.2, 19.6, and 19.9 and substituting into Eq. 19.1 gives

$$P_r = \frac{\beta}{r^4}\frac{\pi\theta\phi r^2 c\tau}{8}\frac{\pi^5}{\lambda^4}|K|^2\sum_{i=1}^{N}D_i^6$$

$$= \frac{\beta\pi^6\theta\phi c\tau|K|^2}{8\lambda^4 r^2}Z \tag{19.10}$$

$$= \frac{\beta' Z}{r^2}$$

This expression illustrates that for the distributed weather target the received power is (1) a function only of β' (a constant dependent upon all the radar system and physical parameters), (2) directly proportional to the radar reflectivity factor Z, and most significant, (3) inversely proportional to r^2 (not r^4 as in the case of point targets).

The radar system parameters included in β in Eq. 19.1 include the peak transmit power P_t, the antenna system gain G twice (once for transmitting and once for receiving), and the wavelength λ. We include all antenna system losses in this antenna system gain factor (radome, waveguide, rotary joints, etc.) since all the measurements must be referenced to the same point in the radar system—usually at a coupler near the circulator. Because the antenna gain is not uniform over the beamwidth, assuming a uniform gain can lead to errors in the calculation of Z. Using a similar derivation, Probert-Jones[34] took this into account, assumed a gaussian shape for the antenna beam, and derived the following equation for the received power:

$$P_r = \frac{P_t G^2\lambda^2\theta\phi c\tau}{512(2\ln 2)\pi^2 r^2}\sum_{i=1}^{N}\sigma_i \tag{19.11}$$

where 2ln2 is the correction for the gaussian-shaped beam. By substituting Eqs. 19.3, 19.6, and 19.7 into Eq. 19.11, the received power can be expressed in terms of the reflectivity factor Z and range r as

$$P_r = \frac{P_t G^2\theta\phi c\tau\pi^3|K|^2 Z}{512(2\ln 2)\lambda^2 r^2} \tag{19.12}$$

Because the receiving filter suppresses some of the received signal power, P_r must be reduced by L_r, which depends on the details of the transmitted spectrum and the receiver filter but is usually a factor of about 1.6 (2 dB) for a typical waveform and "matched filter." Solving for the radar reflectivity factor Z gives

$$Z = [1024\ln 2\ \lambda^2 L_r/P_t G^2\ \theta\phi c\ \tau\pi^3|K|^2]\ P_r r^2 \tag{19.13}$$

where the reflectivity factor is expressed in terms of the received power and range.

One must be careful to use consistent units in Eq. 19.13. If meter-kilogram-seconds (mks) units are used, the calculation of Z will have dimensions of m^6/m^3. Conversion to the more convenient units of mm^6/m^3 requires that Z be multiplied by the factor 10^{18}. Furthermore, expressing P_r and r in common units of dBm (dB relative to 1 milliwatt) and km requires that Z also be multiplied by 10^3. Because Z values of interest can range over several orders of magnitude, a logarithmic scale is often used. Thus,

$$\text{dB}Z = C + P_r\,(\text{dBm}) + 20\log r\,(\text{km}) \tag{19.14}$$

where C (isolated in brackets in Eq. 19.13) is the so called Weather Radar Constant with P_r expressed in dBm and r in km. Typical values of C are 65 to 75 dB for the operational weather radars. It is clear that for fixed range and received power, a lower value of the radar constant C allows a smaller reflectivity value in dBZ to be observed. Thus, smaller values of C correspond to more sensitive radars.

This equation can be used to measure the reflectivity factor Z when the antenna beam is filled, when the small scattering particle Rayleigh approximation is valid, and when the scatterers are in either the ice or the water phase. Because all these conditions are not always satisfied, it is common to use the term Z_e, the effective reflectivity factor, in place of Z. When Z_e is used, it is generally understood that the above conditions are assumed. Practitioners in the field of radar meteorology often use Z_e and Z interchangeably, albeit incorrectly.

Another factor we have ignored in the derivation of the radar equation is attenuation by precipitation and atmospheric gasses. At 10 cm wavelengths the attenuation is usually not significant; however, at 5, 3, and 2 cm and especially the yet shorter mm wavelengths, atmospheric attenuation must be accounted for in the radar equation by adding an additional range dependent term L_a. The following section gives details on estimating this attenuation in commonly encountered conditions.

Finally, it is important to note the Z values are of meteorological significance because they are directly related to cloud properties and actual rainfall rates R as described later in this chapter. Z values in nonprecipitating clouds as small as –40 dBZ are of interest for cloud physics studies. In the optically clear, lower atmospheric boundary layer, "clear air" Z values of the order –20 dBZ to 20 dBZ are typical and frequently originate from insects and birds.[35,36] In rain Z may range from about 0–10 dBZ to as much as 60 dBZ, with a 55 to 60 dBZ rain being of the type that can cause severe flooding. Severe hailstorms may produce Z values higher than 70 dBZ. Many operational radar types are designed to detect those Z values that produce measurable precipitation (0 to 60 dBZ) and "clear air" echoes to 100 km where the Earth's curvature prevents surface-based measurements. Thus, being able to measure strong precipitation echoes at short range and also weak precipitation echoes at long range requires radar receivers having a total dynamic range of 90–95 dB whereas measuring weak echoes in the presence of strong ground clutter requires as large an instantaneous dynamic range (> 60 dB) as possible. More recent operational radars and most research radars attempt to achieve the most sensitivity possible and can detect minimum reflectivity values of –40 dBZ or less at short ranges (e.g., 1 km).

Operational radars in the past have employed sensitivity time control (STC) to reduce gain at short range and compensate for strong nearby echoes; however, recent radars tend not to use STC techniques since receiver dynamic ranges are adequate to cover important weather echo intensities at the necessary ranges. Research radars have rarely used STC owing to the attendant loss of sensitivity at short ranges.

19.3 DESIGN CONSIDERATIONS

Four of the more significant factors that affect the design of meteorological radars are attenuation, range ambiguities, velocity ambiguities, and ground or sea clutter. The combination of these factors, along with the need to obtain adequate spatial resolution, leads to a wavelength selection in the range of 3 to 10 cm for most precipitation based applications.

Attenuation Effects. Attenuation has at least two negative effects on meteorological radar signals. First, making accurate quantitative measurements of the backscattered energy from precipitation at ranges farther than any intervening precipitation becomes very difficult. This inability to precisely measure the true backscattering cross section requires that quantitative measurements of precipitation rates be corrected for attenuation when possible.

Second, if the attenuation due to precipitation or the intervening medium is sufficiently great, the signal from a precipitation cell behind a region of strong absorption may be totally suppressed. One example of the potentially serious consequences of very strong absorption is the impact it might have on aviation storm avoidance radars, most of which are in the 3-cm band. It is common for short wavelength onboard aviation weather radars to not detect intense convective cells behind closer, high attenuation thunderstorms. Severe storms with high precipitation rates also cause high attenuation even at 5-cm wavelengths, as noted by Hildebrand[37] and Allen et al.[38]

In some meteorological radar applications, it is desirable to attempt to measure attenuation along selected propagation paths. This is done because absorption is related to liquid-water content and can provide useful information for the detection of such phenomena as hail, in accordance with the dual-wavelength technique described by Eccles and Atlas[39] and Vivek et al.[40]

In the following subsections, quantitative expressions relating attenuation to precipitation are given. Much of this is taken from Bean, Dutton, and Warner[22] and Lhermitte.[25] Battan[20] and Oguchi[41] are also excellent sources for additional information on the absorbing properties of precipitation.

Attenuation by Water Vapor. Atmospheric water vapor may take on values up to 25 g/m^3 and give variable attenuation depending on the water vapor content. However, at typical weather radar wavelengths longer than 3 cm, the attenuation is less than a few hundredths dB/km and is usually ignored. Gaseous oxygen contributes only a minor absorption effect at these centimeter wavelengths and is also usually ignored.

Attenuation in Clouds. Cloud droplets are regarded here as those water or ice particles having radii smaller than 100 μm (0.01 cm). For wavelengths of incident radiation well in excess of 0.5 cm, the attenuation depends primarily on the liquid-water content and is independent of the drop-size distribution. The generally accepted equations for attenuation by clouds usually show the moisture component of the equations in the form of the liquid-water content (grams per cubic meter). Observations[42] indicate that the liquid-water concentration in clouds generally ranges from 1 to 2.5 g/m^3, although Weickmann and Kampe[43] have reported isolated instances of cumulus congestus clouds (high towering convective clouds that frequently produce heavy precipitation) with water contents of 4.0 g/m^3 in the upper levels. In ice clouds, the water content rarely exceeds 0.5 and is often less than 0.1 g/m^3. The attenuation due to cloud droplets may be written

$$K = K_1 M \tag{19.15}$$

where K = attenuation, dB/km
K_1 = attenuation coefficient, dB/(km · g/m^3)
M = liquid-water content, g/m^3

$$M = \frac{4\pi\rho}{3} \sum_{i=1}^{N} a_i^3 \tag{19.16}$$

$$K_1 = 0.4343 \frac{6\pi}{\lambda} \text{Im}\left(-\frac{m^2 - 1}{m^2 + 2}\right) \tag{19.17}$$

where the a_i are droplet radii, ρ is the density of water, and Im is the imaginary part. Values of K_1 for ice and water clouds are given for various wavelengths and temperatures by Gunn and East[44] in Table 19.1.

Several important facts are demonstrated by Table 19.1. The decrease in attenuation with increasing wavelength is clearly shown. The values change by about an order of magnitude for a change of λ from 1 to 3 cm. The data presented here also shows that attenuation in water clouds increases with decreasing temperature. Ice clouds give attenuations about two orders of magnitude smaller than water clouds of the same water content. The attenuation of microwaves by ice clouds can be neglected for practical purposes.

Attenuation by Rain. Ryde and Ryde[45] calculated the effects of rain on microwave propagation and showed that absorption and scattering effects of raindrops become more pronounced at the higher microwave frequencies, where the wavelengths and the raindrop diameters are more nearly comparable. In the 10-cm band and at shorter wavelengths, the effects are appreciable, but at wavelengths in excess of 10 cm, the effects are greatly decreased. It is also clear that suspended water (cloud) droplets and rain have an absorption rate in excess of that of the combined oxygen and water-vapor absorption.[46]

In practice, it has been convenient to express rain attenuation as a function of the precipitation rate R, which depends on the liquid-water content and the fall velocity of the drops, the latter in turn depending on the size of the drops. Ryde[47] studied the attenuation of microwaves by rain and deduced, by using Laws and Parsons's[48] drop size distributions, that this attenuation in decibels per kilometer can be approximated by

$$K_R = \int_0^{r_0} K[R(r)]^{\alpha} dr \tag{19.18}$$

where K_R = total attenuation, dB
$R(r)$ = rainfall rate along path r
r_0 = length of propagation path, km
K = constant dependent on frequency and temperature
α = constant dependent on frequency

TABLE 19.1 One-way Attenuation Coefficient K_1 in Clouds in dB/km per g/m^3 Liquid Water[44]

		Wavelength, cm			
Temperature, °C		0.9	1.24	1.8	3.2
Water cloud	20	0.647	0.311	0.128	0.0483
	10	0.681	0.406	0.179	0.0630
	0	0.99	0.532	0.267	0.0858
	–8	1.25	0.684	0.34$^+$	0.112$^+$
Ice cloud	0	8.74×10^{-3}	6.35×10^{-3}	4.36×10^{-3}	2.46×10^{-3}
	–10	2.93×10^{-3}	2.11×10^{-3}	1.46×10^{-3}	8.19×10^{-3}
	–20	2.0×10^{-3}	1.45×10^{-3}	1.0×10^{-3}	5.63×10^{-3}

$^+$ extrapolated value

Medhurst[49] shows that $\alpha = 1$ is a good assumption in many cases. The path loss per mile for the three frequency bands of 4, 6, and 11 GHz is shown in Figure 19.1. Lhermitte[25] extends this early work to higher frequencies, confirming the relationship and describing the effect of the drop-size distribution on the attenuation rate. He also reviews more recent empirical data.

The greatest uncertainty in prediction of attenuation rates caused by rainfall, when theoretical formulas are used as a basis for calculation, is the extremely limited knowledge of drop-size distributions in rain of varying fall rates under differing climatic and weather conditions. Lhermitte[25] and Uijlenhoet et al.[50] thoroughly review the evolution of analytic expressions for drop-size distributions, describing the Marshall-Palmer experiment and their resulting exponential distribution and the more general three-parameter Gamma distribution. They also review the dependence of the parameters defining the distribution to the rain rate and to the type of rainfall. There is little evidence that rain with a known rate of fall has a unique drop-size distribution, although Burrows and Attwood's studies seem to indicate that a certain most probable drop-size distribution can be attached to rain of a given rate of fall.[51] Results of this study are shown in Table 19.2, which gives the percentage of total volume of rainfall occupied by raindrops of different diameters and varying rainfall rates (millimeters per hour). In the basis of these results, the absorption cross section of different rain rates is shown in Table 19.3. This table gives the decibel attenuation per kilometer for different rainfall rates for radar wavelengths between 0.3 and 10 cm.

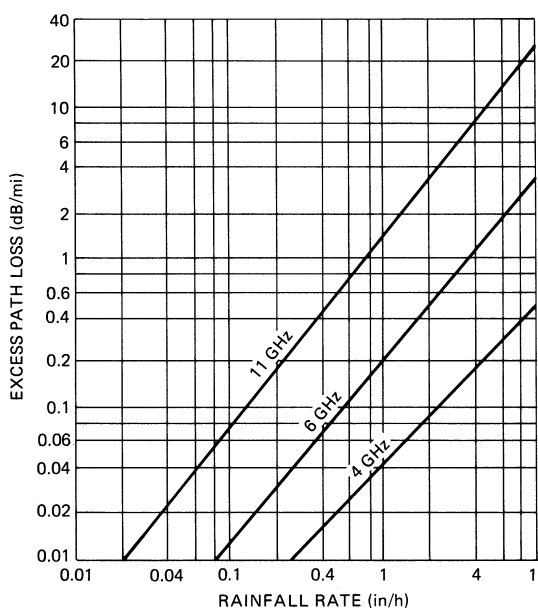

FIGURE 19.1 Theoretical rain attenuation in dB/mile (statute) versus rainfall rate (*after J. W. Ryde and D. Ryde*[45])

TABLE 19.2 Drop Size Distributions at Different Precipitation Rates[51]

	Precipitation Rate R, mm/h							
	0.25	1.25	2.5	12.5	25	50	100	150
Drop Diameter D, cm	Percentage of a Given Volume Containing Drops of Diameter D							
0.05	28.0	10.9	7.3	2.6	1.7	1.2	1.0	1.0
0.10	50.1	37.1	27.8	11.5	7.6	5.4	4.6	4.1
0.15	18.2	31.3	32.8	24.5	18.4	12.5	8.8	7.6
0.20	3.0	13.5	19.0	25.4	23.9	19.9	13.9	11.7
0.25	0.7	4.9	7.9	17.3	19.9	20.9	17.1	13.9
0.30	.....	1.5	3.3	10.1	12.8	15.6	18.4	17.7
0.35	.....	0.6	1.1	4.3	8.2	10.9	15.0	16.1
0.40	.....	0.2	0.6	2.3	3.5	6.7	9.0	11.9
0.45	.....	.....	0.2	1.2	2.1	3.3	5.8	7.7
0.50	.....	.....	.....	0.6	1.1	1.8	3.0	3.6
0.55	.....	.....	.....	0.2	0.5	1.1	1.7	2.2
0.60	.....	.....	.....	.....	0.2	0.5	1.0	1.2
0.65	.....	.....	.....	.....	.....	0.2	0.7	1.0
0.70	.....	.....	.....	.....	.....	.....	.....	0.3

Since the total-attenuation cross section[52] depends on the temperature (because of its effects on the dielectric properties of water), it is important to evaluate the attenuation of rains whose drops are at different temperatures from those in the preceding tables. Table 19.4 contains the necessary data relative to the change of attenuation with temperature and can be used with Table 19.3.

To determine total attenuation caused by rainfall through a particular precipitation path, something must be known or assumed about the nature of the precipitation itself and, consequently, about how its rainfall rates and drop sizes are distributed in three dimensions.

A systematic vertical variation of R, decaying with height above a measured surface value, seems to be appropriate in *stratiform*[53] rainfall, which is rain having a widespread and continuous nature. Such widespread rainfall is usually triggered by

TABLE 19.3 Attenuation in Decibels per Kilometer for Different Rates of Rain Precipitation at a Temperature of 18°C Using the Drop-size Distributions in Table 19.2[51]

Precipitation	Wavelength λ, cm								
Rate R, mm/h	$\lambda = 0.3$	$\lambda = 0.4$	$\lambda = 0.5$	$\lambda = 0.6$	$\lambda = 1.0$	$\lambda = 1.25$	$\lambda = 3.0$	$\lambda = 3.2$	$\lambda = 10$
0.25	0.305	0.230	0.160	0.106	0.037	0.0215	0.00224	0.0019	0.0000997
1.25	1.15	0.929	0.720	0.549	0.228	0.136	0.0161	0.0117	0.000416
2.5	1.98	1.66	1.34	1.08	0.492	0.298	0.0388	0.0317	0.000785
12.5	6.72	6.04	5.36	4.72	2.73	1.77	0.285	0.238	0.00364
25.0	11.3	10.4	9.49	8.59	5.47	3.72	0.656	0.555	0.00728
50	19.2	17.9	16.6	15.3	10.7	7.67	1.46	1.26	0.0149
100	33.3	31.1	29.0	27.0	20.0	15.3	3.24	2.80	0.0311
150	46.0	43.7	40.5	37.9	28.8	22.8	4.97	4.39	0.0481

TABLE 19.4 Correction Factor (Multiplicative) for Rainfall Attenuation[51]

Precipitation Rate R, mm/h	λ, cm	0°C	10°C	18°C	30°C	40°C
0.25	0.5	0.85	0.95	1.0	1.02	0.99
	1.25	0.95	1.00	1.0	0.90	0.81
	3.2	1.21	1.10	1.0	0.79	0.55
	10.0	2.01	1.40	1.0	0.70	0.59
2.5	0.5	0.87	0.95	1.0	1.03	1.01
	1.25	0.85	0.99	1.0	0.92	0.80
	3.2	0.82	1.01	1.0	0.82	0.64
	10.0	2.02	1.40	1.0	0.70	0.59
12.5	0.5	0.90	0.96	1.0	1.02	1.00
	1.25	0.83	0.96	1.0	0.93	0.81
	3.2	0.64	0.88	1.0	0.90	0.70
	10.0	2.03	1.40	1.0	0.70	0.59
50.0	0.5	0.94	0.98	1.0	1.01	1.00
	1.25	0.84	0.95	1.0	0.95	0.83
	3.2	0.62	0.87	1.0	0.99	0.81
	10.0	2.01	1.40	1.0	0.70	0.58
150	0.5	0.96	0.98	1.0	1.01	1.00
	1.25	0.86	0.96	1.0	0.97	0.87
	3.2	0.66	0.88	1.0	1.03	0.89
	10.0	2.00	1.40	1.0	0.70	0.58

a relatively large-scale mechanism, such as a frontal or monsoon situation. A vertical variation of R of the form

$$R = R_0 e^{-dh^2} \tag{19.19}$$

can be assumed to be appropriate under continuous rainfall conditions.[54] R_0 is the surface rainfall rate, h is the height above the Earth's surface, and d is a constant, equal to about 0.2. Convective precipitation, however, shows a quite different nature. For example, the presence of *virga*[53] (precipitation aloft but evaporating before reaching the surface) associated with so many shower-type clouds in dry climates indicates that convective shower rainfall profiles are much more difficult to model.

Attenuation by Hail. Ryde[47] concluded that the attenuation caused by hail is one-hundredth of that caused by rain and that ice-crystal clouds cause no sensible attenuation and show very small attenuation even at the excessive rate of fall of 5 in/h. However, the scattering by ice spheres surrounded by a concentric film of liquid water having a different dielectric constant does not give the same effect that Ryde's results for dry particles would indicate.[55] For example, when one-tenth of the radius of an ice sphere of radius 0.2 cm melts, scattering of 10-cm radiation is approximately 90% of the value that would be scattered by an all-water drop.

At wavelengths of 1 and 3 cm with $2a = 0.126$ (a = radius of drop), Kerker, Langleben, and Gunn[55] found that particles attained total attenuation cross sections corresponding to all melted particles when less than 10% of the ice particles was melted. When the melted

mass reached about 10 to 20%, the attenuation was about twice that of a completely melted particle. These calculations show that the attenuation in the melting of ice immediately under the 0°C isotherm can be substantially greater than in the snow region just above and, under some circumstances, greater than in the rain below the melting level. Further melting cannot lead to much further enhancement, apparently, and may lead to a lessening of the reflectivity of the particle by bringing it to sphericity or by breaking up the particle. Melting of ice particles produces enhanced backscatter, and this effect gives rise to the observed elevated *bright band*[53] near the 0°C isotherm.

Lhermitte[25] discusses hail attenuation for shorter wavelength radars when resonant region (Mie) scattering is the dominant scattering mechanism. Using accepted size distributions of dry hail, he shows attenuation rates over the frequency interval of 3–150 GHz that are negligible at the lower frequencies but rise asymptotically to about 3 dB/km at frequencies above 100 GHz.

Attenuation by Fog. The characteristic feature of a fog is the reduction in visibility. *Visibility*[53] is defined as "the greatest distance in a given direction at which it is just possible to see and identify with the unaided eye (1) in the daytime, a prominent dark object against the sky at the horizon and (2) at night a known, preferably unfocused, moderately intense light source." Although the visibility depends upon both drop size and number of drops and not entirely upon the liquid-water content, in practice the visibility is an approximation of the liquid-water content and, therefore, may be used to estimate radio-wave attenuation.[56]

On the basis of Ryde's work, Saxton and Hopkins[57] give the figures in Table 19.5 for the attenuation in a fog or clouds at 0°C temperature. The attenuation varies with the temperature because the dielectric constant of water varies with temperature; therefore, at 15°C and 25°C the figures in Table 19.5 should be multiplied by 0.6 and 0.4, respectively. It is immediately noted that cloud or fog attenuation is an order of magnitude greater at 3.2 cm than at 10 cm and that nearly another order of magnitude increase occurs between 3.2 and 1.25 cm.

Range and Velocity Ambiguities. Weather radars utilize a sequence of pulses to measure the radar reflectivity and doppler characteristics. Because the pulsing rate typically determines the sampling frequency for doppler quantities on a constant pulsing rate radar, the unambiguous doppler frequency (Nyquist frequency) for a fixed pulse-repetition-frequency (PRF) radar is given by

$$F_{\text{Nyq}} = \pm \text{PRF}/2 \tag{19.20}$$

where PRF is the pulse repetition frequency. Simultaneously, the unambiguous range interval is given by

$$R_a = \frac{c}{2 \cdot \text{PRF}} \tag{19.21}$$

TABLE 19.5 Attenuation Caused by Clouds or Fog Temperature = 0°C[57]

	Attenuation, dB/km		
Visibility, m	$\lambda = 1.25$ cm	$\lambda = 3.2$ cm	$\lambda = 10$ cm
30	1.25	0.20	0.02
90	0.25	0.04	0.004
300	0.045	0.007	0.001

and the product $F_{\text{Nyq}} R_a$ is simply

$$F_{Nyq} R_a = \frac{c}{4} \tag{19.22}$$

Since the doppler shift f and the target radial velocity v are linearly related, the unambiguous velocity is related to the Nyquist frequency by

$$V_a = \frac{\lambda}{2} F_{\text{Nyq}} \tag{19.23}$$

It follows that the product of unambiguous velocity and unambiguous range is

$$V_a R_a = \frac{\lambda c}{8} \tag{19.24}$$

For constant PRF radars, this product is maximized by maximizing λ, the transmitted wavelength. Thus, using longer wavelengths allows optimizing the PRF by trading unambiguous range for unambiguous velocity. For standard constant PRF radars, 10-cm wavelengths have been widely chosen for most precipitation measurements of interest in which design parameters such as radar beamwidth, size of antenna, and attenuation effects may be made acceptable.

Ground Clutter Effects. Many meteorological radar applications call for the detection of precipitation echoes in the presence of ground clutter. Specifically, precipitation measurements near the ground are of extreme interest in agricultural and hydrological applications as well as information for the general public. Applications in which ground clutter is serious relates to the ground-based radar detection of low-level wind shear at airports and measuring precipitation near the ground in mountainous terrain for flash flood warnings. Both the Nexrad and Terminal Doppler Weather Radar (TDWR) network radars have been designed to assure clutter suppression in excess of 40 dB.[7,58]

Although ground clutter cannot be eliminated, its effect can be mitigated through careful design. The primary approach is to use an antenna with low sidelobes, particularly in elevation, which will suppress the clutter component of the input echo when the main beam is slightly above the horizon. A second approach is using shorter wavelengths. Shorter wavelengths result in improved signal-to-clutter ratios owing to the fact that the Rayleigh scattered weather signal power is inversely proportional to λ^4, whereas the ground clutter return is only weakly dependent on wavelength. If one assumes that the clutter signal is wavelength independent and the antenna beamwidth is fixed, it can be shown that the weather-signal-power to clutter-power ratio is inversely proportional to λ^2.

Weather radars typically use digital signal processing techniques to implement clutter filters that suppress near zero velocity clutter echoes.[59] These filters may be implemented using either a time domain clutter filter applied to the I and Q radar video data (one form of which is sometimes called a *delay line canceler* from its early analog implementation) to suppress the zero velocity ground clutter components or a frequency domain doppler power spectrum (a digital "filter bank") to achieve the same effect.[32] The time domain filters for mechanically scanned weather radars are usually infinite impulse response (IIR) filters with narrow, but adjustable, widths up to a few m/s and having suppression levels of 40–60 dB and very steep transition regions.[60] These time domain filters with a frequency notch centered at zero velocity (frequency)

will also suppress weather echo power that may exist in the same velocity region and bias all the estimates of reflectivity, velocity, and width.

Spectral domain clutter filters implemented by a discrete Fourier transform (DFT), on the other hand, suppress the near zero clutter components in the frequency domain and may interpolate the remaining spectrum across this region to retain most of the underlying (signal or noise) spectral information. An alternative frequency domain technique for the Nexrad radar separately models the clutter and weather signal as gaussian-shaped spectra and separates these two components of the doppler spectrum using digital search algorithms and then removes these clutter components while leaving the underlying weather signal unperturbed.[61] Thus, when the gaussian assumptions apply, the remaining weather signal spectrum provides an unbiased estimator for all the weather parameter spectrum moment estimates.

Typical Weather Radar Designs. There is no universal weather radar system design that can serve all purposes. Airborne weather radars are constrained by size and weight limitations. Ground-based radars may be constrained by cost and siting considerations. Severe storm warning radars require long range and high unambiguous velocity and then must penetrate very heavy rain, thus dictating long wavelengths. Radars designed for studies of nonprecipitating clouds typically use short wavelengths[62,63] (8 mm and 3 mm) in order to achieve sufficient sensitivity to detect small cloud particles of the order of 10–100 μm at sufficiently small resolution volumes. Sensitive, short-range FM-CW radars[64] having high average power can be used to obtain very high range resolution for detecting very thin scattering layers in the clear air boundary layer.

Most meteorological radars are pulsed radars having doppler capability. Ground-based radars used for severe storm research and warnings normally use S-band (~3 GHz) or C-band (~5.5 GHz) transmitters. Airborne weather avoidance and precipitation radars primarily use X band (~10 GHz) due to size limitations and occasionally C-band transmitters to minimize attenuation. Airborne and ground cloud radars and spaceborne radars encompass the mm-wavelengths at K_u band (~15 GHz), K_a band (~35 GHz), and W band (~94 GHz).

Beamwidths of ≤ 1° are commonly used for longer-range radars. Admittedly, this is somewhat arbitrary, but the choice of 1° is based upon several decades of experience. A 1° beam will provide a cross-range resolution of 1 km at a range of 60 km. Because thunderstorms contain important spatial features, such as heavy precipitation shafts and updraft cores, with horizontal dimensions of the order 1 to 5 km, a 1° beam is reasonably well matched to these atmospheric phenomena being observed out to ranges of a few hundred km. Shorter-range airborne weather radars often employ beamwidths of 2–3° as a compromise between wavelength requirements and antenna size constraints whereas spaceborne radars may use a fraction of a degree beamwidth to retain usable horizontal resolution at typical long ranges (250–500 km).

Operational weather radars normally are capable of short and long pulse operation in the range of 0.5 μs to about 6 μs and PRFs between 300 and 3000 Hz for long-range precipitation radars. Through pulse-width diversity, high resolution is obtained (usually at short range) whereas for long-range detection, longer pulses provide increased sensitivity and tend to equalize the along-beam and cross-beam resolutions. The shorter wavelength K_u-, K_a-, and W-band radars typically use pulse lengths less than 1 μs to achieve improved range resolution and PRFs between 3000 and 10,000 Hz because of the short-range cloud measurements that are limited by attenuation

at these wavelengths. Space-borne radars also use these higher PRFs but keep track of multiple pulses en-route to their weather regions far below the orbital altitudes.

Equation 19.12 shows that the received power is directly proportional to the pulse length τ. The noise power P_n is conventionally given by

$$P_n = \kappa TB \tag{19.25}$$

where κ = Boltzmann's constant, 1.38×10^{-23} W/(Hz · K)
T = receiver noise temperature, K
B = receiver noise bandwidth, Hz

For a receiver filter matched to the pulse length,

$$B \approx \frac{1}{\tau} \tag{19.26}$$

Sometimes weather radars will use a short pulse for high PRF doppler processing at short ranges and a longer pulse at low PRF for greater sensitivity when performing long-range surveillance scans to monitor distant weather. Since the transmitted peak power is typically constrained to be fixed, then the transmitted average power increases linearly with τ. Also, the matched filter bandwidth and associated noise power decreases inversely with τ. If the radar pulse volume is filled with distributed meteorological scatterers, then the radar cross section of the weather target also increases with τ (as determined by Equations 19.9 and 19.12) and the signal-to-noise ratio (SNR) of received power is proportional to τ^2:

$$\frac{P_r}{P_n} \propto \frac{\tau}{\kappa TB} \approx \frac{\tau^2}{\kappa T} \tag{19.27}$$

Thus, under these common conditions increasing the pulse length will increase the SNR and the effective radar range. It is important to note that the distributed target radar dependence of SNR on τ^2 is different from the point target radar in which the matched filter SNR equals the ratio of pulse energy to noise spectral density ($2E/N_0 = 2P_t\,\tau/N_0$), a linear dependence on τ. The squared dependence for distributed scatterers is because the transmit pulse scatters power from all scatterers in the $c\tau/2$ pulse volume (not just a single point target) thereby increasing the radar cross section of the weather scatterer.

PRFs for meteorological radars range from as low as several hundred s^{-1} for long-range detection to several thousand s^{-1} for shorter-wavelength systems attempting to achieve high unambiguous velocities. Generally speaking, most meteorological doppler radars are operated in a single PRF mode, compromising the radar's ability to unambiguously resolve either range or velocity. However, the pulsing sequence may use a "dual PRF" mode in which groups of constant PRF pulses are transmitted or a "dual (staggered) PRT" (pulse repetition time) to resolve both range and velocity ambiguities.[65] Another approach is to employ a transmitted pulse sequence with random[66] or deterministic[67] phases from pulse to pulse, which allows overlaid echoes to be separated. Multiple PRT techniques have also been explored but are not in common use.[68] Range ambiguities cannot be totally eliminated, but their effects can be significantly mitigated through these approaches.

To discuss design details of the common types of meteorological radars is beyond the scope of this chapter. Rinehart[26] gives a detailed table of system characteristics of

TABLE 19.6 Relevant Nexrad System Characteristics[69]

Transmitted Peak/Average Power (klystron)	750 kW / 1500 W
Pulse length	225, 675 m (1.57, 4.50 μs)
Polarization	Linear horizontal
Wavelength	10.6 cm
Receiver noise temperature	450 K
Dynamic range	95 dB
Antenna gain	45.5 dB
Beamwidth	0.95°
Sidelobe levels	< –27 dB
Maximum range (reflectivity data)	460 km
Maximum range (doppler data)	230 km
Unambiguous velocity	± 50 m/s
Clutter suppression (maximum)	55 dB
System sensitivity	–7.5 dBZ at 50 km
Rotation rate	10–30 deg/sec

a variety of weather radars. However, it will be useful herein to include some of the important characteristics of the Nexrad WSR-88D radar, which illustrate the performance of modern operational weather radars. Table 19.6 contains some of the more relevant original Nexrad design features.

Figure 19.2 shows a typical Nexrad installation at Missoula, Montana. The antenna is mounted on a tower to clear surrounding obstacles such as buildings and trees. The electronic equipment is housed in one shelter and the standby generator is housed in another.

FIGURE 19.2 Nexrad WSR-88D radar at Missoula, Montana, mounted on 15-m tower with two equipment shelters—one containing the transmitter, receiver, processor, and communications equipment, and the other containing a standby generator (*Photo courtesy of NOAA/NWS*)

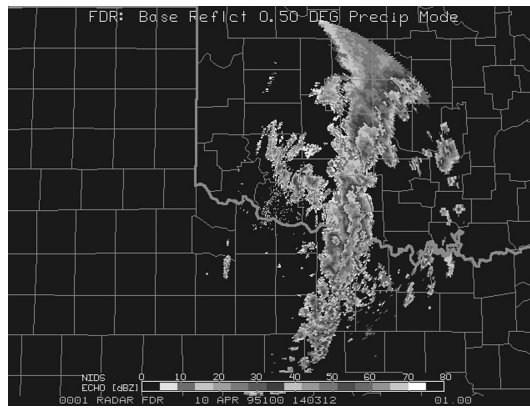

FIGURE 19.3 Nexrad reflectivity data from Frederick, Oklahoma, radar on April 10, 1995, showing line of intense convective cells and surrounding precipitation (*Photo courtesy of NOAA/NWS*)

Figure 19.3 shows an example of radar reflectivity data from the Frederic, Oklahoma, radar as a line of intense thunderstorms and associated rainfall pass through the coverage area. The processing techniques used to generate the various weather images and products are discussed later in this chapter.

Figure 19.4 shows the S-band (10 cm) and K_a-band (0.8 cm) dual-polarization doppler research radar[70] operated by the National Center for Atmospheric Research (NCAR). The system permits simultaneous measurements of the reflectivity factor on two wavelengths, doppler parameters on the S-band wavelength, and extensive polarimetric measurements at both wavelengths. The technical characteristics are similar to the Nexrad specifications. The antenna beams are matched with approximately 1° beamwidth and the large S-band dish is 8.7 m in diameter. The peak transmitted power

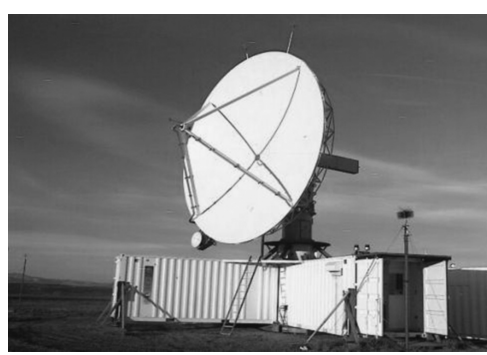

FIGURE 19.4 S-Pol: The multi-parameter S-band and K_a-band polarimetric research radar pointing at the sun for a solar calibration at the National Center for Atmospheric Research, Boulder, Colorado (*Courtesy of University Corporation for Atmospheric Research © 2007, Boulder, CO*)

is 1 MW at S band and 50 KW at K_a band. The pulse widths are approximately 1 μs. The PRF is typically 1000 s^{-1} at S band and a few times larger at K_a band. This radar system is characteristic of the technologies currently in place in the research community.

Polarimetric Radar. Meteorological radars using dual polarization transmit and receive both horizontal and vertical polarizations to estimate additional characteristics of the weather targets.[13,14,24] Transmitting the two orthogonal polarizations either simultaneously (SHV) or transmitting them separately in a predetermined sequence and using dual parallel digital receivers (one on each polarization channel) allow estimation of the differential quantities between echoes from the two polarizations. One can derive improved rainfall rates (as well as other physical information on the type of precipitation) as functions of polarimetric measurements that relate the differences in the horizontally and vertically polarized signals. By far the most common polarimetric parameters are the "differential reflectivity" (Z_{dr}) and "differential phase" (Φ_{dp}), which give bulk scattering and propagation characteristics of the meteorological targets. Letting E_h and E_v denote the complex received signal *voltages* that also represent the received *electric fields* at horizontal and vertical polarizations, the important polarimetric parameters to be estimated are given below[11]:

$$\text{Differential reflectivity } Z_{dr} = \langle Z_h \rangle / \langle Z_v \rangle \tag{19.28}$$

$$\text{Differential phase } \Phi_{dp} = \langle \Phi_v \rangle - \langle \Phi_h \rangle \tag{19.29}$$

$$\text{Specific differential phase } K_{dp} = d\langle \Phi_{dp} \rangle / \text{dr} \tag{19.30}$$

$$\text{Co-polar correlation ratio } \rho_{hv} = |\langle E_h^* E_v \rangle| / \langle E^*_h E_h \rangle^{1/2} \langle E^*_v E_v \rangle^{1/2} \tag{19.31}$$

$$\text{Linear depolarization ratio LDR} = \langle Z_{cx\,v} \rangle / \langle Z_{co\,h} \rangle \tag{19.32}$$

Z_h and Z_v are the measured reflectivities of the horizontal and vertical co-polarized received signals and Z_{dr} is expressed in dB, whereas Φ_h and Φ_v are the measured phases of the same polarized received signals. K_{dp} is the suitably smoothed range derivative of the measured differential phase, Φ_{dp}, and is usually expressed in deg/km. ρ_{hv} is the co-polar correlation coefficient of E_h and E_v where the phase measurements are assumed to be time coincident, which is the case with SHV transmission and reception. LDR is a ratio of the cross-polar vertical reflectivity ($Z_{cx\,v}$) normalized by the co-polar horizontal reflectivity ($Z_{co\,h}$). Because polarimetric measurements add new dimensions of radar information and because these measurements are related to the physical characteristics of the scatterers, suitable combinations of these data give a strong indication of precipitation type (rain, snow, ice particles, sleet, hail, etc)[16,71] as well as radar echo classification into various categories (precipitation, ground or sea clutter, birds and insects, chaff, etc).[72]

Radar Calibration. To effectively use radars for accurate precipitation estimates, the conversion of measured reflectivity factor to received echo power must be well known. The gains (or conversion constants) of the various radar components can be measured using engineering test equipment, manufacturer specifications, and field measurements. Calibrating weather radar usually means to accurately specify the radar constant in the radar equation and to accurately estimate the received power

measured by the radar system. It also encompasses items such as knowing where the scattering volume is in 3D space by knowing antenna pointing angles and accurately determining range.

Although floating spheres, tetrahedral reflectors, and other targets of known radar cross section may be used,[26,73] the important "solar calibration" technique uses the solar position to adjust antenna pointing and the radiated solar flux to determine antenna gain.[74,75] Along with other radar parameter measurements, one can readily determine the radar constant. By injecting test signals of known power, one can determine the receiver gain transfer function. For polarimetric radars special care is required.[76] It has been demonstrated that by measuring the cross-polar powers in addition to the solar flux, an accurate estimate of the differential channel calibration can be obtained.[77] The AMS held a very successful Weather Radar Calibration Symposium[78] documenting all aspects of meteorological radar calibration.

19.4 SIGNAL PROCESSING

To compute the various weather products necessary for forecasting, warning, and other operational activities, the first three spectrum moments corresponding to received power, mean radial velocity, and doppler spectrum or velocity width must be estimated. Keeler and Passarelli[79] review standard estimation techniques and errors for spectrum moment estimation. For the highest resolution measurements, these spectral moments must be computed at each range gate sensed by the radar and converted into meaningful meteorological information. The nature of the distributed meteorological target, which shall be discussed next, imposes some special requirements not generally considered for hard, nonfluctuating targets on the processing techniques to estimate these moments.

It can be shown that the received signal from meteorological targets is well represented by a narrowband gaussian process.[23] This is a direct consequence of the fact that (1) the number of scatterers in the pulse volume is large ($>10^6$); (2) the pulse volume is large compared with the transmitted wavelength; (3) the pulse volume contains multiple point scattering sources, causing all phases on the range from 0 to 2π to be combined and returned; and (4) the particles are in relative motion due to turbulence, wind shear, and their varying fall speeds.

The superposition of the scattered electric fields from such a large number of particles (each with different amplitude and random phase) gives rise, through the central limit theorem, to a signal with bivariate, or a two dimensional, gaussian probability density function. Thus, the fluctuating amplitude of the return signal has a Raleigh statistical distribution and its phase is uniformly distributed between 0–2π. Furthermore, its intensity (power) is exponentially distributed.[80,81] Because all the particles within the sample volume are moving with some mean or average radial velocity, there is a mean frequency of the doppler spectrum that is shifted from the transmitted frequency. Finally, since the particles are in motion with respect to one another, there is also a doppler spread, often referred to as the width of the doppler spectrum. Zrnic describes a straightforward technique of synthesizing digital weather radar signals from a parameterized doppler spectrum characterizing a specific pulse volume.[82] Doviak and Zrnic[23] as well as Bringi and Chandrasekar[24] give detailed derivations of these relationships, whereas Keeler and Passarelli[79] summarize distributed target data characteristics and relate them to the sampled data sets representative of weather radar and other atmospheric sounding systems.

Spectrum Moment Estimation. A common Gaussian model of the mean received power spectral density of a meteorological signal[82] is depicted in Figure 19.5 and can be interpreted as follows. The received power is simply the integral under the curve (the zeroth moment) and is given by

$$P_r = \int S(f)df = \int S(v)dv \tag{19.33}$$

where f and v are related by $f = (2/\lambda)v$.

The mean velocity ($\bar{v}$) is given by the first moment of the spectrum:

$$\bar{v} = \frac{\int vS(v)dv}{\int S(v)dv} \tag{19.34}$$

The spectrum (velocity) width (σ_v) is given by taking the square root of the second central moment:

$$\sigma_v^2 = \frac{\int (v-\bar{v})^2 S(v)dv}{\int S(v)dv} \tag{19.35}$$

Radar meteorologists sometimes refer to σ_v^2 as the spectrum variance because of its computational equivalence to the variance of a continuously distributed random variable. In short, $S(v)$ is analogous to a probability density function for v since it is actually a reflectivity weighted distribution of particle velocities within the scattering volume. The term *spectrum width* will be used to refer to σ_v. It is clear, therefore, that the doppler spectrum contains the information necessary to measure meteorologically important signal parameters. These first three moments are usually referred to as *base data* and often labeled Z, V, and W with the appropriate conversions and units.

In the most general case, quadrature phase detection is used to obtain the real and imaginary parts of the complex signal. These are usually digitized in a large number of range gates (≈1000) at the radar's pulse repetition frequency. The resultant complex time series in each gate can then be processed by using a fast Fourier transform (FFT) to obtain an estimate of the doppler power spectrum[83] from which the echo power, mean velocity, and spectrum width can be obtained.

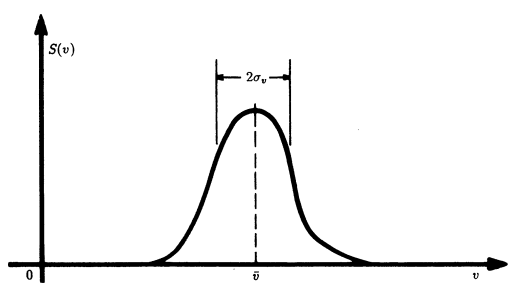

FIGURE 19.5 Gaussian model of the mean doppler power spectrum. The three spectral moments (received power, radial velocity, and spectrum width) can be estimated from the spectrum and are directly related to the meteorological variables of interest.

An efficient moment estimation technique was originally described by Rummler[84] and reinterpreted by Doviak and Zrnic.[23] This estimator makes use of the fact that the complex autocorrelation function of the received signal has the general form

$$R(nT) = P_r\ \rho(nT)\ \exp\left[j\frac{4\pi\bar{v}}{\lambda}nT\right] \tag{19.36}$$

where $\rho(nT)$ is the correlation coefficient of the time series data and nT is the time lag.

It can be shown that $\bar{v}$, the mean velocity, is a function of the first lag $R(T)$

$$\bar{v} = \frac{\lambda}{4\pi T}\arg[R(T)] \tag{19.37}$$

It can also be shown[85] that

$$\sigma_v^2 \approx \frac{\lambda^2}{8\pi^2T^2}\left[1-\frac{R(T)}{R(0)-P_n}\right] \tag{19.38}$$

where P_n is the noise power.

This estimator has been widely used in the past for mean-frequency estimation with doppler meteorological radars. The estimates are unbiased in the presence of noise when the doppler spectrum is symmetrical. Its greatest appeal, however, is due to its computational simplicity. For a pulsed radar, with a pulse repetition period T, $R(T)$ is obtained from adjacent pairs of pulses using the simple expression[86]

$$R(T) = \frac{1}{N}\sum_{k=0}^{N-1} s_{k+1}s_k^* \tag{19.39}$$

where the s_k are the complex in-phase (I) and quadrature (Q) signal samples (sampled at the radar PRT) at a given range and s_k^* is its complex conjugate. It is clear that this algorithm requires N complex multiplications for a time series of N samples whereas the FFT requires $N \log_2 N$. This so-called *pulse-pair algorithm*, therefore, is an efficient spectral moment estimation technique. However, it should be applied only when one is certain to have a pure weather signal in white noise; otherwise, other spectral components or non-white noise will bias the spectral moment estimates.

For many past operational radars, the pulse-pair processor was the technique of choice. However, in many research applications, it remains advantageous for improved data quality control purposes to access the full doppler spectrum and remove artifacts prior to computing the spectral moments corresponding to the meteorological data of interest.[79,87] The wind profiling radar community has made extensive use of spectral processing for artifact removal and sensitivity improvement.[88] One of the more important tasks is estimating the noise floor so as to remove its effect on the spectral moment estimates. Two objective techniques are common.[89,90] Constantly improving programmable digital signal processing chips and signal processing computers make it possible for radar meteorologists to implement various types of spectrum processing techniques that vastly improve data quality over the simple pulse pair processing algorithm. Furthermore, processors that adapt themselves to a variable environment in which they usually operate are feasible. Flexible programming of digital signal processors permits tailoring of the processor's characteristics to the application from day to day or even beam to beam and gate to gate.

Measurement Accuracy. Because the received signals are sample functions from gaussian random processes, the doppler spectrum and its moments cannot be measured exactly in any finite period of time. Consequently, all measurements will be somewhat in error, with the error being a function of the properties of the atmosphere, the radar wavelength, and the time allocated to the measurement.

The theoretical development of signal estimator statistics is found in Denenberg, Serafin, and Peach[91] for the FFT technique. Doviak and Zrnić[23] cover the subject quite completely while Keeler and Passarelli[79] provide a good summary of all these estimation techniques and the respective measurement error expressions. Following are some useful expressions for the mean square error of mean power and mean velocity estimates.

Power Estimation. It is well known[80] that for a gaussian random process using square-law signal detection, samples of the mean power P_r of the process are exponentially distributed with variance P_r^2. The variation is due to the process itself, not any noise associated with the measurement. Given a time T_0 (sec) allocated to the measurement and a signal bandwidth σ_f (Hz), there will be approximately $\sigma_f T_0$ independent samples of the square of the signal envelope. It follows, therefore, that for the high SNR case an estimate of the mean power for this process $\hat{P}_r$ will have a variance or mean square error given by

$$\text{var}(\hat{P}_r) \approx \frac{P_r^2}{\sigma_f T_0} \tag{19.40}$$

Substituting for σ_f from the expression $\sigma_f = 2\sigma_v/\lambda$, where σ_v is the width of the doppler spectrum, Eq. 19.40 becomes

$$\text{var}(\hat{P}_r) \approx \frac{\lambda P_r^2}{2\sigma_v T_0} \tag{19.41}$$

This expression is valid for high signal-to-noise cases.

Velocity Estimation. The variance of the mean frequency estimate of the doppler spectrum is

$$\text{var}(\hat{f}) = \frac{1}{P_r^2 T_0} \int f^2 S^2(f + \bar{f})\, df \tag{19.42}$$

This is an interesting result showing that the variance of the estimate $\hat{f}$ is a function only of the shape of the doppler spectrum (primarily its spectrum width) and the integration time T_0 allocated for processing. If the spectrum can be accurately modeled by a gaussian shape with variance σ_f^2, Eq. 19.42 reduces to

$$\text{var}(\hat{f}) = \frac{\sigma_f}{4\sqrt{\pi} T_0} \tag{19.43}$$

Noting that $\text{var}(\hat{v}) = (\lambda/2)^2 \text{var}(\hat{f})$, we can write

$$\text{var}(\hat{v}) = \frac{\lambda \sigma_v}{8\sqrt{\pi} T_0} \tag{19.44}$$

If we multiply the numerator and denominator by σ_v, Eq. 19.44 becomes

$$\text{var}(v) = \frac{\lambda \sigma_v^2}{8\sqrt{\pi}\,\sigma_v T_0} = \frac{\sigma_v^2}{4\sqrt{\pi}\,\sigma_f T_0} \tag{19.45}$$

Thus, it is seen that the variance of the mean velocity estimate $\hat{v}$ is directly proportional to the variance of the doppler spectrum and inversely proportional to the number of independent samples, $\sigma_f T_0$. Note also that $\text{var}(\hat{v})$ is proportional to λ, indicating that, for the same processing time T_0 and for the same σ_v, the variance of the estimate can be reduced by reducing the wavelength, which increases the number of independent samples.

Equations 19.42–19.45 are applicable in high signal-to-noise ratio cases. Uncertainties in the spectral moment estimates result from the limited observation time of the narrow band random process characterizing the meteorological echo. Any noise in the measurement further increases the uncertainty. Zrnić[85] gives the more general following expression for the variance of the mean frequency estimate f for the pulse-pair estimation technique and a gaussian-shaped spectrum

$$\text{var}(\hat{f}) = \frac{1}{8\pi^2 T_0 \rho^2(T) T}\left\{2\pi^{3/2}\sigma_f T + \frac{N^2}{S^2} + 2\frac{N}{S}\left[1-\rho(2T)\right]\right\} \tag{19.46}$$

where ρ is the correlation coefficient and N/S is the noise-to-signal ratio. Equation 19.46 applies a single PRF with interpulse period T and assumes that all pulses in the interval T_0 are used in the estimation algorithm. It reduces exactly to Eq. 19.43 for a large SNR and for narrow spectra, i.e., $\rho(T) \approx 1$. The reader is referred to Zrnić[85] for further details regarding the estimation of other moments of the doppler spectrum.

Pulse Compression. Pulse compression has been infrequently used for meteorological applications because short pulse peak power has not been a limitation on weather radar system performance. Keeler and Frush,[92] however, described how atmospheric distributed targets may be treated as frozen (fixed) "slabs" of scattering centers such that they approximate layers of nonfluctuating scatterers as the coded radar pulse propagates through them. Thus, each scattering slab produces a return signal that can be compressed by the compression filter in the same way as for individual point targets. They pointed out that pulse compression can benefit rapid-scanning radar applications in which the desired dwell time of each scattering volume is much shorter than the decorrelation time of the weather echoes. In these cases, averaging pulse compressed range measurements, instead of integrating over a longer dwell time, provides the large number of independent samples needed for accurate measurement in a very short beam observation time. Similarly, the effective range resolution over which averaging is performed can be flexible to meet changing observational requirements—short range intervals for highly structured heavy rainfall storms (typically convective) and longer range intervals for more uniform but weaker rainfall (typically stratiform). In other situations where signals are very weak (such as for wind profiler applications and clear air boundary layer observations), pulse compression may be used to increase system sensitivity[93] by increasing the average power of the system using long pulses while processing for any desired range resolution. Range resolution and SNR are independently determined by the pulse compression waveform design parameters.

A note of caution is in order when considering pulse compression for meteorological radars, relating to the matter of range sidelobes. Careful design is necessary to minimize these sidelobes, just as antenna sidelobes should be minimized, in order

to mitigate the effects of interpretive errors caused by wide dynamic range distributed weather targets.[94,95] Amplitude, frequency, and phase shaping of the transmitted pulse along with special sidelobe suppression/compression filters in the receiver processor allow range sidelobes to be suppressed by more than 50 dB over a significant doppler interval—tens of meters per second.[96] These compression filters are not matched to the transmit waveform; therefore, the SNR degrades somewhat and possible loss of range resolution in the main beam may occur.[95] However, these losses are tolerable for many meteorological measurements of interest.

Whitening. Pulse compression involves increased transmit bandwidth that is frequently difficult to have allocated and may limit its use at S band and C band for operational applications. A fixed bandwidth technique for increasing range resolution and the number of independent samples is the process of sampling the transmit pulse at an interval several times shorter than its duration and using a linear predictive *whitening filter*[97] to remove the correlated information from the oversampled data.[98,99] This whitening process increases the number of independent samples for range averaging that allows improved parameter estimation accuracy but at a cost of significantly reduced SNR. The higher noise bandwidth in the receiver required by the higher rate sampling and the whitening filter noise enhancement cause the SNR to be reduced by a factor of approximately L^2 where L is the increased sampling factor.[100] Stated another way, the whitening filter effectively shortens the transmit pulse (by L) while passing the increased receiver noise power (by L) thereby trading range resolution for SNR. Fortunately, for precipitation echoes and typical weather radars, the SNR is quite high, and even after the whitening process, it remains high enough to effectively utilize the larger number of independent samples for improved base data estimates or improved range resolution measurements.[101] On the other hand, if the signal is weak, noise enhancement will dominate the whitening process and any advantage is lost. Highly important is the fact that the transmit pulse and its bandwidth are not changed; consequently, increased frequency allocation to make use of the higher range resolution is not an issue.

Short Dwell Time Spectra (Maximum Entropy). Spectral processing of weather echoes adds another degree of freedom (the frequency dimension) to the ability to discriminate signal from ground clutter, other artifacts, and noise, and to estimate meteorological parameters of interest. Most frequency domain processing requires relatively long IQ data sample sets for discrete Fourier transform analyses, window functions, and possible spectral averaging to obtain spectra suitable for quantitative processing.[102] Faster scanning radars used for sampling rapidly evolving storms requires spectrum analysis techniques that use short dwell time data sets of many fewer IQ data samples. Modern spectrum analysis techniques such as the Burg maximum entropy[103] and the Capon[104] maximum likelihood estimators allow using short dwell sampled data to obtain stable spectrum estimators. These techniques belong to the general class of autoregressive (AR) estimators whereby the observed data are modeled as all-pole filtered white noise rather than a weighted sum of sinusoids according to the Fourier model.[105] Multiple signals and ground clutter may be resolved the same as using Fourier estimators. These short dwell time AR spectra may then be used to estimate weather spectral moments the same as the Fourier data model spectrum estimators from which the weather parameters are derived.[87]

Processor Implementations. Modern meteorological radars use digital signal processing techniques on programmable platforms and interactive color displays

for quantitative precision in interpreting the weather echoes. Modern weather radars require large dynamic range to sense strong echo at short range and weak echo at long range. Thus, the receiver and processor designs attempt to maintain amplitude and phase linearity throughout that range by using a dynamic automatic gain control (AGC), whereby the receiver gain and phase are adjusted along the range interval through the use of rapidly switched attenuators or, more often, digital compensation. Clearly, such rapid switching in the receiver requires careful design in order to avoid the affects of switching transients. An approach that avoids transient effects is to use two parallel IF receiver channels, each with moderate dynamic range and fixed gains, and to sample the signal in the channel that is best matched to the signal strength.

In all those approaches, it is possible to achieve linear dynamic range of greater than 90 dB and to use floating-point digital processing. The reflectivity, mean doppler velocity, and spectrum width can all be estimated digitally from the floating-point samples. The processing can be performed with a dedicated digital signal processing computer or by fast general-purpose computers combined with special signal processing components using Digital Signal Processing (DSP) chips or field programmable gate array (FPGA) devices. Continued technology advances will permit advanced, but mature, signal processing algorithms such as modern spectral processing and adaptive filtering to be implemented.[87]

19.5 OPERATIONAL APPLICATIONS

As has been demonstrated, meteorological radars measure backscattered power and radial velocity parameters. The challenge to the radar meteorologist is to translate these measurements, their spatial distributions, and their temporal evolution into quantitative assessments of the weather. Serafin and Wilson,[1] among others, show how modern meteorological radars are used for forecasting the weather. The level of sophistication used in interpretation varies broadly, ranging from human interpretation of rudimentary displays to automatic algorithms and modern multidimensional displays to assist human interpretation. Expert system approaches[106,107] that attempt to reproduce human interpretive logical processes have been employed effectively. The degree to which automation can be applied is evident in the Nexrad radar system design that produces the automated meteorological products shown in Table 19.7.

TABLE 19.7 Partial List of Nexrad Automated Products

Base radar reflectivity (all ranges, each scan)
Base radial velocity
Base spectrum width
Composite (maximum at all heights) reflectivity
Precipitation echo tops
Severe weather probability
Velocity Azimuth Display (VAD) Wind Profile
Storm relative mean radial velocity
Vertical integrated liquid
Storm tracking information
Hail potential
Mesocyclone and Tornado Vortex Signature
Surface rainfall accumulation (1 hr, 3 hr, total storm)
Radar Echo Classifier

Precipitation Measurement. Among the more important parameters to be measured is rainfall, having significance to a number of water resource management problems related to agriculture, fresh-water supplies, storm drainage, and warning of potential flooding. The rainfall rate can be empirically related to the reflectivity factor by an expression of the form[108]

$$Z = aR^b \tag{19.47}$$

where a and b are constant and R is the rainfall rate, usually in millimeters per hour. Battan[20] devotes three full pages of his book to the listing of dozens of Z-R relationships derived by investigators at various locations throughout the world, for various weather conditions, and in all seasons of the year. The fact that no universal expression can be applied to all weather situations is not surprising when one notes that rainfall drop-size distributions are highly variable. For many conditions, the drop-size distribution can be represented by an exponential function

$$N(D) = N_0 e^{-\Lambda D} \tag{19.48}$$

where N_0 and Λ are constants and $\Lambda D_0 = 3.67$ where D_0 is the median drop diameter. If $N(D)$ is known, the reflectivity factor can be calculated from Eq. 19.8. By using the terminal-fall speed data of Gunn and Kinzer,[109] the rainfall rate can also be obtained and Z related to R as shown in Eq. 19.47. The exponential form of the drop-size distribution generally fits the average of several drop-size distributions that occur over different phases of convective and tropical rainfall and are averaged over space or time. However, the "gamma" drop-size distribution represents a better fit to instantaneous, natural variations of the drop-size distribution under different conditions. The gamma drop-size distribution[24] is given as

$$N(D) = N_0 D^{\mu} e^{-\Lambda D} \tag{19.49}$$

with $\mu > -1$ and $\Lambda D_0 = 3.67 + \mu$. The μ parameter controls the shape of the distribution and when $\mu = 0$, the distribution is exponential.

Clearly, a single-wavelength, single-polarization radar can measure only a single parameter Z and must assume Rayleigh scattering. Since the rainfall rate depends upon two parameters, N_0 and Λ, it is not surprising that Eq. 19.47 is not universal. Despite this fact, Battan[20] lists four expressions as being "fairly typical" for the following four types of rain:

$$\text{Stratiform rain}[110]\ Z = 200\ R^{1.60} \tag{19.50}$$

$$\text{Orographic rain}[111]\ Z = 31\ R^{1.71} \tag{19.51}$$

$$\text{Thunderstorm rain}[112]\ Z = 486\ R^{1.37} \tag{19.52}$$

$$\text{Snow}[113]\ Z = 2000\ R^{2.00} \tag{19.53}$$

Stratiform[53] refers to widespread, relatively uniform rain and uses the well-known Marshall-Palmer drop-size distribution. *Orographic*[53] rain is precipitation that is induced or influenced by hills or mountains, whereas *Thunderstorm*[53] rain is typical of convective precipitation systems. In each of the above expressions, Z is in mm^6/m^3 and R is in mm/h. In Eq. 19.53, R is the precipitation rate of the water-equivalent melted snow. Battan[20] gives a more complete treatment of this important topic.

Wilson and Brandes[114] give a comprehensive treatment of how radar and rain-gauge data can be used to complement one another in measurements of precipitation over large areas. They state that the radar determined storm cumulative precipitation measurements are expected to be accurate within a factor of 2 for 75% of the time. Accuracies over large areas can be improved to about 30% with the addition of a surface rain-gauge network. Although radar measures reflectivity aloft, the primary concern is rainfall estimation at the surface. Rain gauge measurements are frequently used to adjust the radar reflectivity values.[115] Zawadzki[116] describes many factors that influence rainfall measurement by radar. Joss and Lee[117]and others[118,119,120] use the Vertical Profile of Reflectivity (VPR) to estimate the surface rainfall rate with some success. Bridges and Feldman[121] discuss how two independent measurements (reflectivity factor and attenuation) can be used to obtain both parameters of the drop-size distribution and more precisely determine the rainfall rate.

Polarimetric Estimates. Dual polarization radar has been proven to yield improved rainfall estimates as well as other advantages for weather radar.[122] Polarimetric radar measurements take advantage of the flattened raindrop shape approximated by an oblate spheroid (a flattened sphere having a horizontal dimension greater than its vertical dimension), and its propagation and scattering characteristics, to obtain accurate rain-rate estimators. Seliga and Bringi[123] and Sachidananda and Zrnic[124] show how the co-polar measurements of Z at horizontal (Z_h) and vertical (Z_v) polarizations can produce two independent measurements and, therefore, provide more accurate rainfall-rate measurements than those related to simple reflectivity. Bringi and Chandra[24] give the following rain-rate estimators for measurements at 10 cm (S band). Other wavelengths have different constants because of Mie factors entering into the calculations and the wavelength dependence of phase measurements.

$$R(Z_h, Z_{dr}) = 0.0067\ Z_h^{\ 0.93}\ Z_{dr}^{\ -3.43} \tag{19.54}$$

$$R(K_{dp}) = 50.7\ K_{dp}^{\ 0.85} \tag{19.55}$$

$$R(K_{dp}, Z_{dr}) = 90.8\ K_{dp}^{\ 0.93}\ Z_{dr}^{\ -1.69} \tag{19.56}$$

The reflectivity-based rain-rate estimators corresponding to the Marshall-Palmer ($Z = 200R^{1.6}$) and the common Nexrad WSR-88D ($Z = 300R^{1.4}$) relations are

$$R_{MP}(Z) = 0.0365\ Z^{0.625} \quad \text{for Marshall-Palmer} \tag{19.57}$$

$$R_{88D}(Z) = 0.0170\ Z^{0.714} \quad \text{for Nexrad WSR-88D} \tag{19.58}$$

The polarimetric precipitation measurements bring unique characteristics that address not only improved precipitation measurements, but also improved data quality characteristics.[125] The differential reflectivity between the horizontal and vertical polarizations (Z_{dr}) allows estimating the effective drop size, whereas differential phase (K_{dp}) gives additional, somewhat independent information on estimation of rainfall rates. K_{dp} is an especially important parameter when the radar is confronted with typical contaminants as beam blockage, ground clutter domination, and calibration errors. Furthermore, Ryzhkov and Zrnic[126] have shown that K_{dp}-based rainfall measurements are less dependent on the unknown and variable drop-size distribution (DSD) than power-based measurements. Furthermore, other inferences from the

polarimetric measurements allow one to estimate the parameters of the gamma function form of the DSD,[127] which may further improve rainfall estimation. And, self consistency constraints of the polarimetric precipitation covariance matrix impose relatively strict bounds on the absolute reflectivity measurements, allowing one to calibrate the reflectivity measurement and make improved rainfall rate estimates.[128] For short wavelength radars, one must consider Mie scattering effects when measuring rainfall rate by reflectivity measurement. Lhermitte[25] and Kollias et al.[129] give an analysis of Mie scattering and show that if the scattering is properly accounted, the rainfall measurements are accurate.

Polarimetric radars may be configured in different ways for different measurements. Research radars explore the depolarization ratios by alternating horizontally and vertically polarized pulses. However, the preferred configuration for operational radars is to transmit both horizontal and vertical polarizations simultaneously while independently receiving both orthogonal signals for polarimetric processing, allowing reception of the important co-polar quantities. The relative phase of each transmitted polarization is arbitrary, but the differential magnitude and phase of the co-polar received signals in each polarization are sufficient for the polarimetric measurements.

It is our opinion that no single topic in radar meteorology has received more attention than rainfall rate measurement. Although useful empirical expressions have evolved and dual-polarization techniques show significant improvements in accuracy, a completely satisfactory approach remains to be developed.

Polarimetric measurements by the WSR-88D radars will allow more accurate precipitation measurements and ice-water phase knowledge that is important for making improved forecasts, separating winter precipitation into regions of rain and snow, and detecting hazardous aircraft icing conditions.[130] Implementation of phase-coding algorithms allow these radars to separate multiple time around (or multiple trip) echoes[67,131,132] and to compute dealiased velocities in the range dealiased echoes[133]; to classify and separate precipitation echoes from artifacts as ground clutter, sea clutter, and insects echoes[72]; to accommodate flexible scan strategies; and to incorporate improved data resolution in range and azimuth. These performance enhancements are readily achieved by installing greater and more flexible signal and data processing power.

Severe Storm Warning. One of the primary purposes of weather radars is to provide timely warnings of severe weather phenomena such as tornadoes, damaging winds, flash floods, and landfalling hurricanes. Accurate long-term forecasting of the precise location and level of severity of these phenomena, through data assimilation and numerical weather prediction techniques, is beyond the present state of the art. Operational radars, however, can detect these phenomena and provide local warnings of approaching severe events; they can also detect the rotating mesocyclones in severe storms that are precursors to the development of tornadoes at the Earth's surface.[134] Ground-based coastal and airborne radars can also measure the severity of approaching hurricanes and define their most intense landfall positions for evacuation warnings.[135,136]

Tornado Detection. A single doppler radar can measure only the radial component of the vector wind field. Hence, exact measurements of vector winds at a point are generally not possible. However, rotating winds or vortices can be detected and

their intensities measured by simply measuring the change in radial velocity with azimuth angle, as shown in Figure 19.6. The radar scans in azimuth and detects a couplet in radial velocity at constant range. The azimuth shear is given simply by the expression

$$\frac{dv_r}{dx} \approx \frac{2v_r}{r\alpha} \tag{19.59}$$

where x is in the direction orthogonal to the radius of the circulation and α is the angle subtended by the circulation at range r.

Because mesocyclones may spawn tornadoes and can be many kilometers in diameter, radars with about 1° beamwidth have the spatial resolution to detect mesocyclones at ranges in excess of 60 km. It should be clear that any mean translational motion would change the absolute values of the measured radial velocities but would not affect the shear measurement. Azimuthal shear values of the order of 10^{-2} s^{-1} or greater and with vertical extent greater than the diameter of the mesocyclone are deemed necessary for a tornado to occur.[137]

Detection of the tornado vortex itself is not generally possible beyond about 30 km using typical weather radar beamwidths, since its horizontal extent may be only a few hundred meters. Detection of the radial shear, therefore, is not possible unless the tornado is close enough to the radar to be resolved by the beamwidth. However, in cases where the tornado falls entirely within the beam, the doppler spectrum width may be used to estimate tornadic intensity. In some cases, both a mesocyclone and its incipient tornado can be detected. Wilson and Roesli[138] show an excellent early example of a tornado vortex signature (TVS) embedded within a larger mesocyclone.

Microbursts. Fujita and Caracena[139] first identified the microburst phenomenon as the cause of an airliner crash that took place in 1975. The microburst and its effects on an aircraft during takeoff or landing are depicted in Figure 19.7. The microburst is simply a small-scale, short-duration downdraft emanating from a convective storm. This "burst" of air spreads out radially as it strikes the ground, forming a ring of *diverging*[53]air about 0.3 to 1 km deep and of the order of 2 to 4 km in diameter with divergent winds greater than 10 m/s and lasting less than 20 minutes. Aircraft penetrating a microburst first experience an increase in head wind and then a continuous, performance-robbing decrease in head wind, which can cause the plane to crash if encountered shortly before touchdown or just as the aircraft is taking off. More complete descriptions of microbursts and their effects on aviation safety are given by Fujita[140,141] and McCarthy and Serafin.[142]

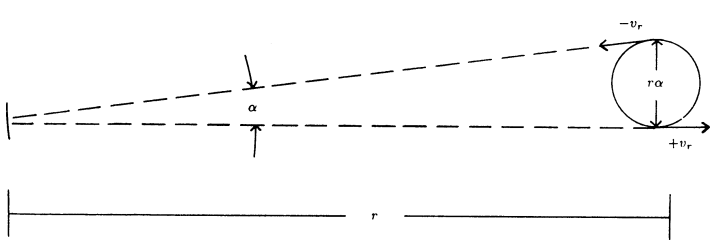

FIGURE 19.6 Measurement of rotation or azimuthal wind shear in a mesocyclone, a rotating wind parcel. The azimuthal shear is given by $\Delta v/\Delta x = 2v_r/r\alpha$. (*Courtesy of University Corporation for Atmospheric Research © 2007, Boulder, CO*)

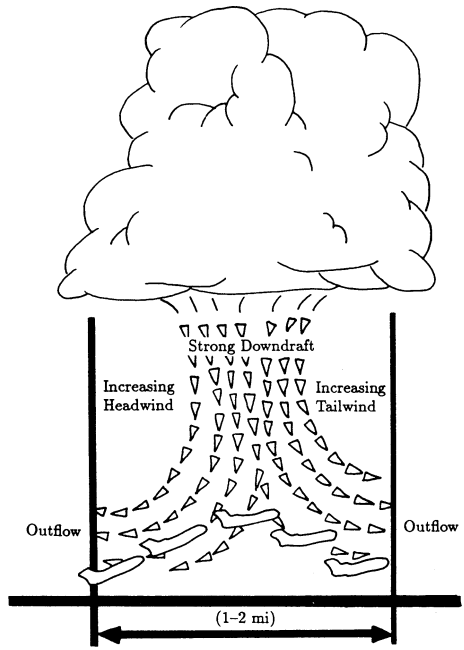

FIGURE 19.7 Depiction of a microburst and its effect on an aircraft during takeoff. The loss of airspeed in the divergent wind field near to the ground is extremely hazardous. A similar loss of airspeed near the ground occurs during landing. (*Courtesy of University Corporation for Atmospheric Research © 2007, Boulder, CO*)

Microburst detection, like tornado detection, is accomplished by estimating shear. However, in the case of the microburst, it is the radial shear of the radial velocity that is typically measured. Human interpretation of microburst signatures in color-enhanced radial velocity displays is easily accomplished with trained observers[50] and automatic detection has been implemented on the TDWR radar system. Radial velocity differences of 10 to 50 m/s are observed in microbursts. A radial velocity difference of more than 25 m/s over the length of a jet runway (≈3 km) is a serious concern.

One principal problem concerning microbursts is their short lifetimes, which are on the order of 15–20 minutes but the duration of peak intensity is only 1 or 2 minutes. Field research[143] has clearly demonstrated that a few minutes advance warning using doppler radar can be achieved. Operational microburst detection radars use this automated detection algorithm with high performance ground clutter mitigation techniques since the phenomenon occurs near the ground and oftentimes in very light or no precipitation.

C band is the preferred operational frequency for several reasons. First, a C-band antenna will have a smaller beamwidth than an S-band antenna of the same size and allow improved air flow measurements with strong clutter suppression near the airport surface. Second, since short range detection is important, radar attenuation effects are not a primary concern. Third, C band offers improved signal-to-clutter

performance since the large clutter targets are limited in radar cross section by Mie scattering, whereas the atmosphere-borne wind tracing scatterers are small and obey Rayleigh scattering cross section physics. X-band radars have been considered to some degree but the more severe attenuation that can occur in very heavy rain will limit performance unless the radar is located very near to the airport runways. In the mid-1990s the C-band Terminal Doppler Weather Radar (TDWR) system was installed at 45 major airports to detect and warn aircraft of hazardous wind shear conditions, approaching gust fronts that may affect the airport approach and departure configuration, and microbursts.[7] This network of radars along with much improved pilot training and awareness has all but eliminated aircraft accidents caused by microbursts and strong wind shear.

Hail. The Nexrad radar makes use of a hail-detection algorithm that combines a high reflectivity factor with echo height and upper-level divergent radial velocity winds to detect the occurrence of hail. Polarimetric radar techniques improve quantitative hail detection. Bringi et al.,[15] Aydin et al.,[144] and Illingworth et al.[145] proposed a hail detection technique using differential reflectivity measurements. This technique depends upon the fact that for tumbling hail the differential reflectivity, the ratio of horizontal to vertical reflectivity, is near unity (≈0 dB). This differs sharply from heavy rain, where this ratio can be as large as 5 dB because large water droplets are horizontally oriented. The combination of absolute reflectivity factor and the dual polarization differential reflectivity gives unique signatures for hail and heavy rain, each of which is characterized by a high reflectivity factor. The difference in the differential reflectivity signatures is easily explained. Large raindrops assume flatter shapes (approximated by oblate spheroids) as they fall and thus scatter back the horizontally polarized electric field more strongly than the vertically polarized electric field. Hailstones, having an irregular shape, physically tumble while they fall and, therefore, exhibit no preferred orientation on average. Thus, the horizontal and vertical scattered fields have nearly the same average value.

Wind Measurement. Lhermitte and Atlas[146] were the first to show how a single doppler radar can be used to measure vertical profiles of the horizontal wind field when precipitation is present. This technique is most accurate if the wind field is uniform in the region scanned by the radar. The method depends upon an analysis of the radial velocity measured during a complete scan in azimuth with a single fixed elevation angle. At any slant range r, the height of the measurement is $r \sin \alpha$ and the radius of the region scanned is $r \cos \alpha$, where α is the elevation angle as depicted in Figure 19.8. If β is the azimuth angle, V_h is the horizontal wind speed, and V_f is the fall speed of the particles, then the radial velocity at range r is given by

$$V_r(\beta) = V_h \cos \beta \cos \alpha + V_f \sin \alpha \tag{19.60}$$

A harmonic analysis (least square fitting the amplitude, phase, and offset of a sinusoid) can be used to obtain V_h, the horizontal wind speed, the wind direction where cos β is maximum, and V_f, the mean particle fall speed all plotted as a function of height. This technique is referred to as the Velocity-Azimuth-Display (VAD). Browning and Wexler[147] later showed how the VAD technique could be extended to measure other parameters of the wind field including wind-field divergence and wind-field deformation by employing an extended harmonic or Fourier series analysis. The VAD has been implemented on the Nexrad as a standard product that can be used in precipitation and

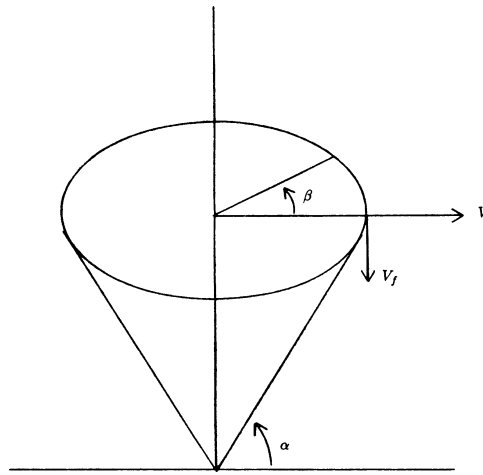

FIGURE 19.8 Velocity-Azimuth-Display geometry for measuring horizontal wind with a single doppler radar. Measurement of the radial velocity for a complete azimuthal scan (β) at elevation angle α permits an estimate of the vertical profile of horizontal winds. (*Courtesy of University Corporation for Atmospheric Research © 2007, Boulder, CO*)

frequently in clear air. The VAD technique is most often applied to wind profiler radars that point vertically and step scan at relatively large elevation angles. An alternative determination of boundary layer wind fields using a single weather radar has found success using an echo tracking technique.[148]

Thunderstorm Prediction. Wilson and Schreiber[149] illustrate how meteorological doppler radar can be used to detect locations where new thunderstorm development is likely to occur. Many weather radars have sufficient sensitivity to detect discontinuities of clear air echoes in the lower 2 to 4 km of the atmosphere out to 50 or 100 km. This detection occurs principally in the summer months when the backscattering mechanism is caused by insects in the lower levels of the atmospheric boundary layer and sometimes may also be due to Bragg-scattered refractive index inhomogeneities. Wilson and Schreiber have found that about 90% of the thunderstorms that occur in the Front Range of the Rockies in the summertime develop over such "boundaries" between two different air masses. Since these boundaries can be detected before any clouds are present and it is possible to infer the air mass convergence (or coming together of two air masses) where insects are forced to accumulate along these boundaries by doppler radar measurements, more precise prediction of thunderstorm occurrence is possible. From the radar designer's standpoint, such applications dictate the use of antennas with very low sidelobes (along with low-phase noise transmitters and receiver components) and signal processors having significant ground clutter rejection capability. The Nexrad radar system, with its high quality antenna and 50 dB of clutter rejection, is well suited to this important operational task.

Refractivity and Water Vapor Measurements. Conventional weather radar processing is generally designed to emphasize precipitation and wind-field measurements

and to suppress ground clutter. However, it is known that radar beam bending caused by atmospheric refraction and the resulting anomalously propagated ground clutter echo gives an indication of the vertical profiles of temperature and moisture in the intervening lower atmosphere. Moreover, measuring the propagation speed of the radar pulse between normally propagated clutter targets (those directly viewed by the radar) gives an estimate of the refractive index of air along this propagation path. By measuring the absolute phase of the radar signal received from stationary ground clutter targets and comparing them with reference absolute phase measurements under known refractive conditions, one can measure the near surface propagation speeds of the radar pulse along these paths. Then, the refractive index, or refractivity, of the atmosphere of these atmospheric paths may be determined.[17] Refractivity is a function of temperature, pressure, and moisture content. Consequently, if surface temperature and pressure are independently available, as they frequently are, then the refractive index measurements may be converted to spatial fields of water vapor in the surface boundary layer. Such water vapor measurements are critical for obtaining accurate forecasts using numerical models and simulations of the atmosphere.[150] This experimental measurement technique can be used to ranges of about 40 km where the Earth's curvature prevents routine observation of ground clutter targets and is being considered for operational use in Nexrad.

19.6 RESEARCH APPLICATIONS

Operational meteorological radars are designed for reliability and simplicity of operation while providing the performance needed for operational applications. Research radars are considerably more complex, since cutting-edge research requires more detailed and more sensitive measurements of a multiplicity of variables simultaneously. In the research community, multiple-parameter (polarization and wavelength) radar studies, multiple doppler radar network studies, and a new generation of airborne and spaceborne radars are receiving considerable attention.

Dual Polarization/Wavelength Radar. It is clear that polarimetric doppler radars provide a significant increase in the useful information that can be obtained from meteorological targets. The detection of hail and more accurate rainfall estimates has primary significance. Dual polarization measurements at multiple wavelengths provide even more information related to the eventual interpretation of the size distributions, water-phase states, and hydrometeor (water or ice particles) types in different classes of precipitation and clouds. The capabilities of multiple-parameter meteorological radars are presented in Bringi and Hendry,[14] Bringi and Chandra,[24] and in the collection of papers edited by Hall.[151] Whereas longer-wavelength radars are necessary for the study of severe storms, shorter wavelength millimeter-wave radars are useful for sensing and probing newly developing clouds. Researchers often need a wide range of these capabilities simultaneously. From the radar engineering standpoint, the challenge is considerable, requiring radar designers to develop coherent waveform, polarization-diverse, and wavelength-diverse radars. As noted, there exist several polarimetric research radars and operational radars in the world.[26]

Multiple Radars. A single doppler radar measures only a single radial component of velocity. Lhermitte[152] was among the first to describe how two or more doppler radars could be used, scanning together, to obtain the full three-dimensional air motion

fields in precipitation. This pioneering work led the way toward the use of networks of doppler radars for studies of individual clouds to examine the three-dimensional structure of vector air motion in precipitation. A point should be made here regarding the use of two doppler radars for measurements of three-dimensional winds. Since, in principle, two independent looks can measure only two components of vector air motion, the assumption of atmospheric mass continuity is invoked. This *equation of mass continuity*[53] ($\nabla \cdot \bar{V} = 0$) is used to obtain the third-dimensional component, where $\bar{V}$ is the vector air motion and is constrained to be zero at the surface. The vertical air motion is calculated from vertical integration of the mass continuity equation.

Figure 19.9 illustrates an air motion field obtained by two doppler radar observations in an individual convective storm cell. Shown are the horizontal vector fields in a plane approximately 100 m above the surface. The phenomenon being measured is a low-level divergent outflow (or microburst) just to right of the center. Figure 19.10 shows another example of precipitation intensity and air motion fields superposed on a photograph of a convective thunderstorm cell. The data are taken from three doppler radars spaced about 40 km apart.

A developing network of short range doppler radars not range limited by the Earth's curvature will provide more detailed observations close to the surface than the relatively widely spaced WSR-88D network. The Collaborative, Adaptive Sensing of the Atmosphere (CASA) radar network will include many inexpensive, low power, scanning, short wavelength radars mounted on towers of opportunity, primarily cell phone towers that blanket much of the U.S.[153,154] Existing equipment on these towers will

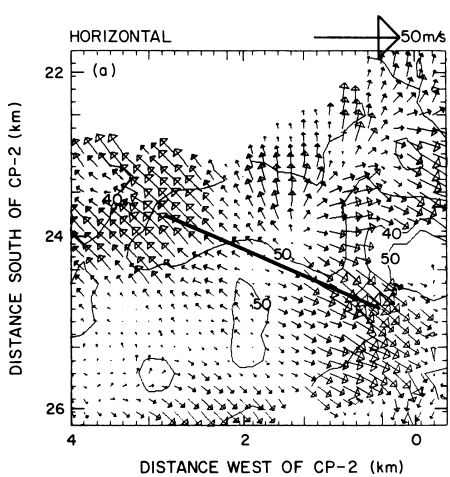

FIGURE 19.9 Vector wind fields in a horizontal plane derived from dual-doppler radar observations of a summertime convective storm near Denver, Colorado. The dark, solid line is shown to indicate the length of a typical jet aircraft runway. The divergent outflow from a microburst shows a strong 15 m/s headwind changing to a similarly strong tailwind over the length of the runway. CP-2 is the former research radar operated by NCAR. (*Courtesy of University Corporation for Atmospheric Research © 2007, Boulder, CO*)

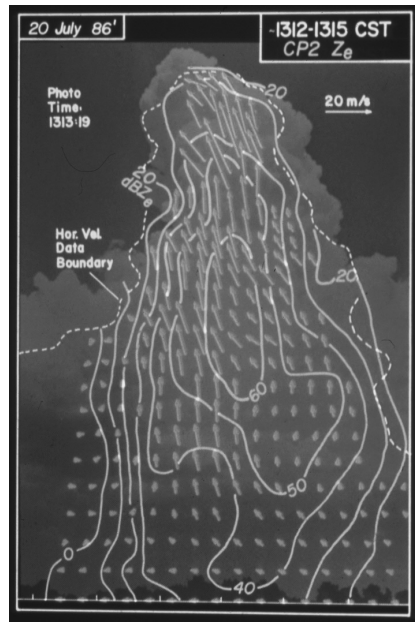

FIGURE 19.10 Radar reflectivity contours and air flow vectors superposed on photograph of a rapidly growing Alabama thunderstorm cell. The data depicts a 30 m/s updraft originating in an extremely strong 60 dBZ rain or hail core. The wind vectors are taken from combining data from three nearby doppler radars. (*Courtesy of American Meteorological Society. From D.E. Kingsmill and R. M. Wakimoto, "Kinematic, Dynamic, and Thermodynamic Analysis of a Weakly Sheared Severe Thunderstorm over Northern Alabama,"* Monthly Weather Review, *vol. 119, p. 272, 1991*)

provide a shared infrastructure for the CASA radars. This radar system will include intelligent decision making for scanning and tracking important low-level atmospheric features that are deemed critical for the aviation, weather forecasting, transportation, and local emergency response users. The CASA radars can communicate with each other for collaborative use of the data and adaptively change their operating parameters to best meet the prescribed needs at a given time. Depending on the final costs of deployment and operation, CASA networks may be developed only around critical areas such as urban areas, airports, etc.

Rapid Scan (Phased Array) Radar. Doppler weather radars that use phased array antennas and complex waveform design may be applied to some of the more difficult radar meteorology observations. The use of multiple doppler radars has provided dramatic new information on the internal winds in large precipitating systems—information that can be obtained in no other way. Despite the power of this technique, the spatial resolution in the derived three-dimensional motion fields is generally not better than

of the order of 1 km. There are several reasons for this. The finite beamwidth limits the resolution available at longer ranges. At shorter ranges, the large solid angle that must be scanned in order to cover all regions of a storm requires total scanning times of the order of 3 to 5 min even for well-situated storms. This is a consequence of the on-target dwell time necessary for accurate measurements. Finally, the storm itself is evolving and moving during this measurement time, thus complicating the data registration in space and time.

Some operational and many research applications require faster scanning than conventional mechanically scanned radars can provide.[155] These applications include longer lead times for tornado warnings, the study of finer scale storm features, interactions between the internal motions and hydrometeor growth processes in the storms, and studies of electric charge separation in clouds. Brook and Krehbiel[156] were among the first to discuss a very rapid-scanning radar (although nondoppler) for effectively obtaining snapshots of convective storms. Keeler and Frush[157] discuss design considerations for a more capable rapid-scanning doppler radar.

Any rapid-scanning approach generally must encompass two features: (1) the transmit waveform must have a relatively large bandwidth to increase the number of independent samples available in the desired spatial resolution cell; and (2) the antenna must be rapidly scanned throughout the desired atmospheric volume either mechanically or electronically. Mechanically scanned single frequency (standard) weather radars use a long dwell time to acquire an adequate number of independent samples to accurately estimate the spectral moment data used for meteorological measurements. A large bandwidth system (e.g., pulse compression radar) can acquire independent samples in range in a short dwell time that can be averaged, thus reducing the dwell time for each beam and reducing the total volume coverage scan time. Fast mechanical scanning (>60 deg/sec) produces deleterious spectrum broadening effects[157] that electronic step scanning easily avoids since the beam is fixed in space during the dwell time. A favored approach is to utilize a one-dimensional phased array that is electronically scanned in elevation while slowly rotating in azimuth.[158] In this way, a full hemispheric volume can be covered in 1–2 minutes and smaller sector volumes may be covered in less than 1 minute.[159] Several military radars and aviation radars utilize electronically scanned beams but the expense of a fully capable system has prevented more than only a few meteorological radar systems from being designed and built.[160,161] Rapid-scanning phased array radars have also been studied extensively in Europe.[162]

An alternative approach is to employ digital beamforming or frequency-steering techniques to transmit and simultaneously receive multiple beams using parallel receivers. Such military radars have been operated for several decades[163] but none of these systems were ever designed or used for weather measurements. A mechanically scanned multiple beam weather radar system using simultaneous frequency scanned beams has been designed and constructed on a small truck. The Rapid Doppler on Wheels (Rapid-DOW) X-band radar, shown in Figure 19.11, uses six simultaneous frequency-steered beams separated by a few degrees emanating from a slotted waveguide phased array and independent receivers to acquire a volumetric coverage of convective storms in 1–3 minutes.[164] Pulse compression is not used. The rapid data acquisition speed of this system has the potential to give new insights into thunderstorm evolution, hurricanes at landfall, hail formation plus microburst, gust front and tornado genesis mechanisms that may likely evolve into an operational capability.

In the early 1990s, the FAA led an effort to develop dual-use weather and aircraft surveillance radar based on electronic scanning and pulse compression techniques,[165]

FIGURE 19.11 Rapid-DOW (Doppler on Wheels) is a mobile X-band radar that uses six simultaneous beams to cover a volume of atmosphere in a much shorter volume coverage time than a mechanically scanned single beam radar. This rapid update scan is important for measuring violent convective storms, especially tornadoes as shown in photo. (*Photo courtesy of University Corporation for Atmospheric Research © 2007, Boulder, CO*)

and an effort beginning a decade later continued the development of phased array radars for civil applications.[166] Radars initially designed for military applications were modified for weather detection and successfully demonstrated the concept.[167] In the early 2000s, a joint effort between the U.S. Navy, the National Weather Service, the National Severe Storms Laboratory, and the University of Oklahoma led to the development of the so-called National Weather Radar Testbed facility in Norman, Oklahoma, by combining a single panel SPY-1 phased array radar on a rotating pedestal with a WSR-88D transmitter and custom receiver.[168] Although this particular radar is not likely to be the preferred design for a future weather radar, the Oklahoma Phased Array Radar testbed can be used to explore electronic scanning strategies together with new pulsing and processing concepts that may lead to future development of a phased array weather radar system.

Airborne Radars. Whereas commercial aviation weather radars are nose mounted X-band radars for severe weather and turbulence detection and avoidance, airborne research radars must have relatively more complex architectures[169] in order to make more sensitive, high-resolution measurements. This powerful technique permits the use of a mobile platform, which therefore allows measurements over regions not accessible by ground-based systems. Moreover, the mobility of the aircraft permits longer term observations of rapidly moving but long-lived storms and cloud systems, thereby allowing more complete studies of evolution during various phases of the system.[170]

NCAR's Eldora airborne doppler radar system,[171] shown in Figure 19.12, consists of two slotted waveguide fixed-beam antennas mounted in the tail of the P-3 aircraft, which is operated by the Naval Research Laboratory and covered by a rotating

FIGURE 19.12 Tail-mounted ELDORA doppler weather radar operated by the National Center for Atmospheric Research on the Naval Research Laboratory P-3 research aircraft (*Courtesy of University Corporation for Atmospheric Research © 2007, Boulder, CO*)

radome—a roto-dome. One beam points forward about 18° and the other aft by the same angle, thereby obtaining two radial components of common target volumes. With such a system, each antenna scans in a conical surface—one cone pointing forward, the other one rearward—thus permitting synthesis of a dual-doppler radar system along the aircraft track. The aircraft is flown alongside storms to synthesize dual-doppler observations and, therefore, to obtain vector winds. Because the aircraft need not fly orthogonal tracks, the time required for measurements of cloud systems is dramatically reduced as are the errors in these measurements. Moreover, severe storms (which could otherwise not be penetrated along an orthogonal track) and hurricanes (which can be penetrated by such aircraft) can be observed fully by an aircraft outside the regions of severe weather.

Various airborne radars exist in the research community for different applications and user groups. NASA has developed the dual wavelength (3 cm and 3 mm) EDOP radar for the high altitude ER-2 aircraft[172] and a W-band 94-GHz airborne cloud radar for the DC-8 research aircraft.[173] NOAA has operated two X-band radars similar to the ELDORA radar for hurricane tracking and research.[174] JPL developed the ARMAR radar[175] to test space radar concepts for the Tropical Rainfall Measurements Mission (TRMM). The University of Wyoming uses a 3-mm cloud radar mounted on a King Air aircraft.[176] In the mid-2000s, NCAR acquired the High-performance Instrumented Airborne Platform for Environmental Research (HAIPER, a Gulf Stream G-5 medium-size jet aircraft) and designed a dual wavelength (8 and 3 mm) removable pod-mounted radar for cloud studies.[177] The Canadian National Research Council has developed a similar airborne radar system.[178]

Spaceborne Radars. Among the more significant challenges facing researchers today is the need to make global measurements of precipitation. Understanding global climate requires that quantitative measurements of precipitation be made throughout the world, particularly in the tropics and over the oceans. Satellite observations appear

to offer the only practical mechanism for obtaining these measurements. The TRMM satellite was launched in 1997 carrying the K_u-band single frequency Precipitation Radar (PR)[179] and a 2.4 m single beam array antenna that is steered 17° on either side of the spacecraft track. Its relatively low inclination orbit at 350 km altitude provides tropical precipitation measurements with 250 m range resolution and a 4.5 km footprint over a 250 km swath. A TRMM follow-on program, the Global Precipitation Measurement (GPM) program, envisions extending precipitation coverage to the mid-latitude (65° *N* and *S* latitude) flying in a 250 km altitude orbit and using dual wavelength precipitation radar (DPR)[180] at K_u and K_a bands for more accurate rainfall estimates using attenuation techniques.[181,182] The two radars will have matched beams from two slotted waveguide array antennas and provide coverage under the spacecraft track similar to TRMM.

CloudSat is a satellite launched in 2006 flying a W band (3 mm) cloud profiling radar (CPR) orbiting the Earth in a sun synchronous orbit at an altitude of about 700 km.[183] The transmitter is an Extended Interaction Klystron (EIK) high-power amplifier generating a 3.3 μsec monochromatic pulse having peak power of 1.7 kW. The antenna is a 1.85 m diameter reflector offset fed by a quasi-optical transmission line and produces a 0.12° beam with extremely low sidelobes. These radar design parameters allow an exceptional sensitivity of –26 dBZ at the Earth surface. CloudSat orbits in formation with four other satellites as part of the so-called A-train constellation of satellites that provide combined radar, lidar, and radiometric measurements for Earth studies. The CPR on-board CloudSat has 500 m vertical resolution with a 1.4 km footprint and is similar to the NASA Airborne Cloud Radar that has flown for several years on board the NASA DC-8 aircraft[173]. Combining these high-resolution cloud measurements with high sensitivity is one of the technical goals for acquiring new information regarding cloud effect on the Earth's climate.

Clear-Air Wind Profiling Radars. Another form of doppler radar that has become widely used, especially in the research community, is the so-called wind profiling radar,[10] or "wind profiler." Wind profilers usually take the form of VHF and UHF multiple fixed-beam systems, pointing vertically and at angles approximately 15° from the zenith to infer profiles of the horizontal wind averaged over the area of measurement. Such radars can make doppler measurements throughout the range of altitudes from a few hundred meters to 20 km or more above the surface, depending upon the wavelength selected and the power-aperture product available. These radars have the ability to measure high resolution winds continuously, which permits the observation of smaller scale temporal and spatial wind-field features that cannot be obtained from the global 12-hour rawinsonde (balloon launch) network. These smaller scale measurements are important for understanding local and regional weather and for effective forecasting on these scales.

Very powerful radars of this type are referred to as Mesosphere, Stratosphere, Troposphere (MST) radars because of their ability to make measurements throughout most of these atmospheric regions up to 60–100 km in altitude. Several major MST radar facilities located at facilities around the world operate at VHF frequencies around 50 MHz and observe upper atmospheric (tropospheric and lower stratospheric) winds or the higher level stratospheric and mesospheric winds. Shorter wavelength UHF wind profilers operating at 400–450 MHz sense atmospheric winds up to 20–25 km and these "tropospheric wind profilers" are the most widely used for operational weather observations. UHF wind profilers operating at 915 MHz in the U.S. and 1200–1300 MHz

in Europe cover the lower atmospheric winds up to 3–5 km (or a few km higher with larger antennas) where the strong moisture fluctuations present in the atmospheric boundary layer provide strong scattering signatures at these shorter wavelengths. These UHF boundary-layer wind profilers are typically used for air pollution monitoring and warnings as well as various research applications.

These clear-air radars receive energy backscattered from refractive index inhomogeneities caused by naturally occurring atmospheric turbulence.[184] The antenna systems usually take the form of phased arrays that form beams several degrees wide that are switched to 3, 4, or 5 nearly vertical beams for 1–2 minutes each and measure vertical profiles of wind every 5–30 minutes. The antennas are frequently of the coaxial collinear (co-co) style for those radars and Yagi array elements for those at the higher frequencies. The higher frequency UHF profilers typically use either Yagi or microstrip patch array antennas. Transmitters are generally in the form of high-powered, coherent transmitting tubes or solid-state amplifiers. At the University of Kyoto, Japan, the antenna-transmitter system consists of 475 crossed Yagi radiating elements, each with its own solid-state transmitter.[185] This approach allows for very flexible electronic scanning of the beam. NOAA operates a network of over thirty 404 and 449 MHz wind profilers in the central United States using solid-state transmitters that supply continuous wind profiles up to 20 km for improved weather forecasts and current upper air wind information for aviation applications.[186]

It is important to recognize that three-beam doppler systems can accurately measure horizontal winds in all three velocity components if the wind is uniform. Four- and five-beam systems allow one to determine the quality of the measurements by detecting the presence of a nonuniform wind flow. Carbone, Strauch, and Heymsfield[187] and Strauch et al.[188] address the issue of wind measurement error in detail. The reader is referred to the review paper by Röttger and Larsen[10] for a thorough treatment of wind-profiler technology and to the sequence of Tropospheric Profiling Symposia for tropospheric profiling applications of winds and other meteorological parameters.[189]

Spaced Antenna Techniques. An additional advantage of these long wavelength radars is their ability to measure not only the radial vertical wind components directly, but also the mean horizontal wind that is transverse to the vertical beam without scanning that beam off zenith. These profilers use the so-called spaced antenna techniques with multiple receivers to process the amplitude and phase differences of the echo structures as they translate over two adjacent antennas (usually subarrays of the same array antenna) to measure components of the horizontal or transverse wind.[190] In this manner, two orthogonal subarrays can measure components of the horizontal wind using cross-spectral or correlation processing techniques.[191] Since the measurement is made in pairs of overlapping beams directly above the radar, it is no longer necessary to assume or require horizontal homogeneity of the wind field in the larger area above the radar and/or the long integration times necessary to assure this homogeneity. These spaced antenna techniques are most frequently used when high spatial and temporal resolution measurements are required such as estimating detailed boundary layer turbulence fields. Zhang and Doviak have investigated using the dual beam–spaced antenna technique implemented with an electronically scanned phased array radar to estimate the transverse, as well as the radial, wind components at arbitrary scan angles.[192]

REFERENCES

1. R. J. Serafin and J. W. Wilson, "Operational weather radar in the United States: Progress and opportunity," *Bull. Am. Meteorol. Soc.*, vol. 81, pp. 501–518, AMS, Boston, 2000.
2. R. J. Serafin, "New nowcasting opportunities using modern meteorological radar," in *Proc. Mesoscale Analysis Forecast. Symp.*, European Space Agency, Paris, 1987, pp. 35–41.
3. T. D. Crum and R. L. Alberty, "The WSR-88D and the WSR-88D Operational Support Facility [Now Radar Operations Center]," *Bull. Am. Meteorol. Soc.*, vol. 74, pp. 1669–1687, 1993.
4. T. D. Crum, R. E. Saffle, and J. W. Wilson, "An update on the Nexrad program and future WSR-88D support to operations," *Weather and Forecasting*, vol. 13, pp. 253–262, 1998.
5. J. McCarthy, J. Wilson, and T. T. Fujita, "The Joint Airport Weather Studies (JAWS) project," *Bull. Am. Meteorol. Soc.*, vol. 63, pp. 15–22, 1982.
6. M. Michelson, W. W. Shrader, and J. G. Wieler, "Terminal doppler weather radar," *Microwave J.*, vol. 33, pp. 139–148, 1990.
7. J. G. Wieler and W. W. Schrader, "Terminal Doppler Weather Radar (TDWR) system characterizations and design constraints," in *25th Int. Conf. on Radar Meteorol.* AMS, 1991, pp. J7–J9.
8. National Research Council, *Assessment of Nexrad Coverage and Associated Weather Services*, Washington, DC: National Academy Press, 1995.
9. H. W. Baynton, R. J. Serafin, C. L. Frush, G. R. Gray, P. V. Hobbs, R. A. Houze, Jr., and J. D. Locatelli, "Real-time wind measurement in extratropical cyclones by means of doppler radar," *J. Appl. Meteorol.*, vol. 16, pp. 1022–1028, 1977.
10. J. Röttger and M. F. Larsen, "UHF/VHF radar techniques for atmospheric research and wind profiler applications," Chapter 21 in *Radar in Meteorology*, Atlas (ed.) Boston: AMS, 1990, pp. 235–281.
11. V. Chandrasekar, R. Meneghini, and I. Zawadzki, "Global and local precipitation measurements by radar," Chapter 9 in *Radar in Atmospheric Science: A collection of essays in honor of David Atlas*, R. Wakimoto and R. Srivastava (eds.), Meteorological Monograph, vol. 30, Boston: AMS, 2003, pp. 215–236.
12. J. Wurman, J. Straka, E. Rasmussen, M. Randall, and A. Zahrai, "Design and deployment of a portable, pencil-beam, pulsed, 3-cm doppler radar," *J. Atmos. Oceanic Technol.*, vol. 14, pp. 1502–1512, 1997.
13. D. S. Zrnic, "Weather radar polarimetry: Trends toward operational applications," *Bull. Amer. Meteorol. Soc.*, vol. 77, pp. 1529–1534, 1996.
14. V. N. Bringi and A. Hendry, "Technology of polarization diversity radars for meteorology," Chap. 19 in *Radar in Meteorology*, Atlas (ed.), Boston: AMS, 1990, pp. 153–189.
15. V. N. Bringi, T. A Seliga, and K. Aydin, "Hail detection with a differential reflectivity radar," *Science*, vol. 225, pp. 1145–1147, 1986.
16. J. Vivekanandan, D. S. Zrnic, S. M. Ellis, R. Oye, A. V. Ryzhkov, and J. Straka, "Cloud microphysics retrieval using S-band dual polarization radar measurements," *Bull. AMS*, vol. 80, pp. 381–388, 1999.
17. F. Fabry, C. Frush, I. Zawadzki, and A. Kilambi, "On the extraction of near-surface index of refraction using radar phase measurements from ground targets," *J. Atmos. Ocean. Tech.*, vol. 14, pp. 978–987, 1997.
18. P. H. Hildebrand and R. K. Moore, "Meteorological radar observations from mobile platforms," Chapter 22 in *Radar in Meteorology*, Atlas (ed.), Boston: AMS, 1990, pp. 287–322.
19. R. J. Serafin and R. Strauch, "Meteorological radar signal processing in 'air quality meteorology and atmospheric ozone,'" *American Society for Testing and Materials*, pp. 159–182, Philadelphia, 1977.
20. L. J. Battan, *Radar Observation of the Atmosphere*, Chicago: University of Chicago Press, 1973.
21. D. Atlas (ed.), *Radar in Meteorology*, Boston: AMS, 1990.
22. B. R. Bean, E. J. Dutton, and B. D. Warner, "Weather effects on radar," in *Radar Handbook*, 1st Ed., M. Skolnik (ed.), New York: McGraw-Hill Book Company, 1970, pp. 24-1–24-40.

23. R. J. Doviak and D. S. Zrnić, *Doppler Radar and Weather Observations*, 2nd Ed., Mineola, NY: Dover Publications, 2006.
24. V. N. Bringi and V. Chandrasekar, *Polarimetric Doppler Weather Radar: Principles and Applications*, Cambridge, UK: Cambridge Univ. Press, 2001.
25. R. M. Lhermitte, *Centimeter & Millimeter Wavelength Radars in Meteorology*, Miami: Lhermitte Publications, 2002.
26. R. E. Rinehart, *Radar for Meteorologists*, 4th Ed., Columbia, MO: Rinehart Publications, 2004.
27. "Special issue on radar meteorology," *IEEE Trans. Geosci. Electron*., GE-17, IEEE, October 1979.
28. R. M. Wakimoto and R. C. Srivastava (eds.), *Radar and Atmospheric Science: A Collection of Essay in Honor of David Atlas*, Meteorological Monographs, Vol. 30, Boston: AMS, 2003.
29. P. Meischner (ed.), *Weather Radar: Principles and Advanced Applications*, Berlin: Springer-Verlag, 2004.
30. *Preprints and Proceedings of Conferences on Radar Meteorology*, 1947–present, Boston: AMS.
31. *Proceedings of European Conferences on Radar in Meteorology and Hydrology,* 2000–present, Berlin, Germany: Copernicus GmbH.
32. M. I. Skolnik, *Introduction to Radar Systems*, 3rd Ed., New York: McGraw-Hill, 2001, p. 772.
33. G. Mie, "Beiträge zur Optic trüber Medien, speziell kolloidaler Metallösungen [Contribution to the optics of suspended media, specifically colloidal metal suspensions]," *Ann. Phys.*, vol. 25, pp. 377–445, 1908.
34. J. R. Probert-Jones, "The Radar Equation in Meteorology," *Q. J. R. Meteorol. Soc.*, vol. 88, pp. 485–495, 1962.
35. J. W. Wilson, T. M. Weckwerth, J. Vivekanandan, R. M. Wakimoto, and R. W. Russell, "Boundary layer clear air radar echoes: origin of echoes and accuracy of derived winds," *J. Atmos. Oceanic Technol.*, vol. 11, pp. 1184–1206, 1994.
36. R. W. Russell and J. W. Wilson, "Radar-observed fine lines in the optically clear boundary layer: reflectivity contributions from aerial plankton and its predators," *Boundary Layer Meteorol.,* vol. 82, pp. 235–262, 1997.
37. P. H. Hildebrand, "Iterative correction for attenuation of 5 cm radar in rain," *J. Appl. Meteorol.*, vol. 17, pp. 508–514, 1978.
38. R. H. Allen, D. W. Burgess, and R. J. Donaldson, Jr., "Severe 5-cm radar attenuation of the Wichita Falls storm by intervening precipitation," in *19th Conf. Radar Meteorol.*, AMS, Boston, 1980, pp. 87–89.
39. P. J. Eccles and D. Atlas, "A dual-wavelength radar hail detector," *J. Appl. Meteorol.*, vol. 12, pp. 847–854, 1973.
40. R. E. Carbone, D. Atlas, P. Eccles, R. Fetter, and E. Mueller, "Dual wavelength radar hail detection," *Bull. Amer. Meteor. Soc.*, vol. 54, pp. 921–924, 1973.
41. T. Oguchi, "Electromagnetic wave propagation and scattering in rain and other hydrometeors," *Proc. IEEE*, vol. 71, pp. 1029–1078, 1983.
42. R. J. Donaldson, Jr., "The measurement of cloud liquid-water content by radar," *J. Meteorol.*, vol. 12, pp. 238–244, 1955.
43. H. K. Weickmann and H. J. aufm Kampe, "Physical properties of cumulus clouds," *J. Meteorol.*, vol. 10, pp. 204–221, 1953.
44. K. L. S. Gunn and T. W. R. East, "The microwave properties of precipitation particles," *Q. J. R. Meteorol. Soc.*, vol. 80, pp. 522–545, 1954.
45. J. W. Ryde and D. Ryde, *Attenuation of Centimeter Waves by Rain, Hail, Fog, and Clouds*, Wembley, England: General Electric Company, 1945.
46. B. R. Bean and R. Abbott, "Oxygen and water vapor absorption of radio waves in the atmosphere," *Geofts, Pura Appl.*, vol. 37, pp. 127–144, 1957.
47. J. W. Ryde, "The attenuation and radar echoes produced at centimetre wavelengths by various meteorological phenomena," in *Meteorological Factors in Radio Wave Propagation*, London: Physical Society, 1946, pp. 169–188.

48. J. O. Laws and D. A. Parsons, "The relationship of raindrop size to intensity," in *24th Ann. Meet. Trans. Am. Geophys. Union*, 1943, pp. 452–460.
49. R. G. Medhurst, "Rainfall attenuation of centimeter waves: comparison of theory and measurement," *IEEE Trans. Ant. Prop.,* vol. AP-13, pp. 550–564, 1965.
50. R. Uijlenhoet, M. Steiner, and J.A. Smith, "Variability of raindrop size distributions in a squall line and implications for radar rainfall estimation," *J. Hydrometeorol.*, vol. 4, pp. 43–61, 2003.
51. C. R. Burrows and S. S. Attwood, *Radio Wave Propagation, Consolidated Summary Technical Report of the Committee on Propagation, NDRC*, New York: Academic Press, 1949, p. 219.
52. W. J. Humphreys, *Physics of the Air*, New York: McGraw-Hill Book Company, 1940, p. 82.
53. *Glossary of Meteorology*, 2nd Ed., Boston: AMS, 2000, p. 885.
54. D. Atlas and E. Kessler III, "A model atmosphere for widespread precipitation," *Aeronaut. Eng. Rev.*, vol. 16, pp. 69–75, 1957.
55. M. Kerker, M. P. Langleben, and K. L. S. Gunn, "Scattering of microwaves by a melting spherical ice particle," *J. Meteorol*., vol. 8, p. 424, 1951.
56. A. C. Best, *Physics in Meteorology*, London: Sir Isaac Pitman & Sons, Ltd., 1957.
57. J. A. Saxton and H. G. Hopkins, "Some adverse influences of meteorological factors on marine navigational radar," *Proc. IEE (London)*, vol. 98, pt. III, p. 26, 1951.
58. J. N. Chrisman and C. A. Ray, "A first look at the operational (data quality) improvements provided by the Open Radar Data Acquisition (ORDA) system," in *21st Int. Conf. on Infor. Processing Sys. (IIPS) for Meteorol., Oceanog., and Hydrol.*, San Diego, CA, P4R.10, 2005.
59. M. Sachidananda and D. S. Zrnic, "Clutter filtering and spectral moment estimation for doppler weather radars using staggered pulse repetition time (PRT)," *J. Atmos. Ocean. Tech.*, 17, pp. 323–331, 2000.
60. L. B. Jackson, *Digital Filters and Signal Processing*, 2nd Ed., Norwell, MA: Kluwer, 1989.
61. A. D. Siggia and R. E. Passarelli, Jr., "Gaussian model adaptive processing (GMAP) for improved ground clutter cancellation and moment calculation," in *3rd European Conf. on Radar Meteoro.*, Visby, Island of Gotland, Sweden, 2004, pp. 67–73.
62. F. Pasqualucci, B. W. Bartram, R. A. Kropfli, and W. R. Moninger, "A millimeter-wavelength dual-polarization doppler radar for cloud and precipitation studies," *J. Clim. Appl. Meteorol.*, vol. 22, pp. 758–765, 1983.
63. R. Lhermitte, "A 94-GHz doppler radar for cloud observations," *J. Atmos. Ocean. Technol.*, vol. 4, pp. 36–48, 1987.
64. J. H. Richter, "High-resolution tropospheric radar sounding," *Proc. Colloq. Spectra Meteorol. Variables, Radio Sci.*, vol. 4, pp. 1261–1268, 1969.
65. R. J. Keeler, D. S. Zrnic, and C. L. Frush, "Review of range velocity ambiguity mitigation techniques," in *29th Conf. on Radar Meteorol.*, AMS, Montreal, 1999, pp. 158–163.
66. B. G. Laird, "On ambiguity resolution by random phase processing," in *20th Conf. Radar Meteorol.*, Boston, AMS, 1981, p. 327.
67. M. Sachidananda and D. S. Zrnic, "Systematic phase codes for resolving range overlaid signals in a doppler weather radar," *J. Atmos. Oceanic Technol.,* vol. 16, pp. 1351–1363, 1999.
68. J. Pirttilä and M. Lehtinen, "Solving the range-doppler dilemma with the SMPRF pulse code," in *30th Conf. Radar Meteorol.*, Munich, AMS, 2001, pp. 322–324.
69. National Research Council, *Weather Radar Technology beyond Nexrad*, Washington, DC: National Academy Press, 2002.
70. R. J. Keeler, J. Lutz, and J. Vivekanandan, "S-Pol—NCAR's polarimetric doppler research radar," in *Proc. Int. Geosci. Remote Sens. Symp. [IGARSS 2000]*, IEEE, Honolulu, 2000, pp. 1570–1573.
71. H. Liu and V. Chandrasekar, "Classification of hydrometeors based on polarimetric radar measurements: development of fuzzy logic and neuro-fuzzy systems and in-situ verification," *J. Atmos. Ocean. Technol.*, vol. 17, pp. 140–164, 2000.

72. C. J. Kessinger, S. M. Ellis, and J. VanAndel, "The radar echo classifier: a fuzzy logic algorithm for the WSR-88D," presented at *83rd AMS Annual Meeting (3rd AI Conf.)*, P1.6, Long Beach, 2003.
73. D. Atlas, "Radar calibration: some simple approaches," *Bull. Am. Meteorol. Soc.*, vol. 83, pp. 1313–1316, 2002.
74. J. F. Pratt and D. G. Ferraro, "Automated solar gain calibration, preprints," in *24th Conf. Radar Meteorol.*, AMS, Tallahassee, 1989, pp. 619–622.
75. D. Sirmans and B. Urell, "On measuring WSR-88D antenna gain using solar flux," NWS ROC Engineering Branch Report, 2001.
76. E. Gorcucci, J. Scarchilli, and V. Chandrasekar, "Calibration of radars using polarimetric techniques," *IEEE Trans. Geosci. Rem. Sens.*, vol. 30, pp. 853–858, 1992.
77. J. C. Hubbert, V. N. Bringi, and D. Brunkow, "Studies of the polarimetric covariance matrix. Part I: Calibration methodology," *J. Atmos. Ocean. Technol.*, vol. 20, pp. 696–706, 2003.
78. Radar calibration workshop presented at *81st Annual Meeting of the Am. Meteorol. Soc.*, Albuquerque, 2001.
79. R. J. Keeler and R. E. Passarelli, "Signal processing for atmospheric radars," Chapter 20 in *Radar in Meteorology*, Atlas (ed.), Boston: AMS, 1990, pp. 199–229.
80. J. S. Marshall and W. Hitschfeld, "The interpretation of the fluctuating echo for randomly distributed scatterers," Pt. I, *Can. J. Phys.*, vol. 31, pp. 962–994, 1953.
81. P. R. Wallace, "The interpretation of the fluctuating echo for randomly distributed scatterers," Pt. II, *Can. J. Phys.*, vol. 31, pp. 995–1009, 1953.
82. D. S. Zrnic, "Simulation of weather-like doppler spectra and signals," *J. Appl. Meteorol.*, vol. 14, pp. 619–620, 1975.
83. D. S. Zrnic and R. J. Doviak, "Velocity spectra of vortices scanned with a pulse-doppler," *J. Appl. Meteorolo.*, vol. 14, pp. 1531–1539, 1975.
84. W. D. Rummler, "Introduction of a new estimator for velocity spectral parameters," *Tech. Memo MM-68-4121-5*, Bell Telephone Laboratories, Whippany, NJ, 1968.
85. D. S. Zrnić, "Estimating of spectral moments for weather echoes," *IEEE Trans. Geosc. Electron.*, vol. GE-17, pp. 113–128, 1979.
86. A. V. Oppenheim and R. W. Schaefer, *Digital signal processing*, Englewood Cliffs, NJ: Prentice-Hall, 1975.
87. F. Fabry and R. J. Keeler, "Innovative signal utilization and processing," Chapter 8 in *Radar in Atmospheric Science: A Collection of Essays in Honor of David Atlas,* R. Wakimoto and R. Srivastava (eds.), Meteorological Monographs, Vol. 30, Boston: AMS, 2003, pp. 199–214.
88. T. L. Wilfong, D. A. Merritt, R. J. Lataitis, B. L. Weber, D. B. Wuertz, and R. G. Strauch, "Optimal generation of radar wind profiler spectra," *J. Atmos. Ocean. Technol.,* vol. 16, pp. 723–733, 1999.
89. P. H. Hildebrand and R. H. Sekhon, "Objective determination of the noise level in doppler spectra," *J. Appl. Meteorol.*, vol. 13, pp. 808–811, 1974.
90. H. Urkowitz and J. P. Nespor, "Obtaining spectral moments by discrete Fourier transform with noise removal in radar meteorology," *Proc. Int. Geosci. Remote Sens. Symp. [IGARSS-92]*, IEEE, Houston, 1992, pp. 125–127.
91. J. N. Denenberg, R. J. Serafin, and L. C. Peach, "Uncertainties in coherent measurement of the mean frequency and variance of the doppler spectrum from meteorological echoes," in *15th Conf. Radar Meteorol.*, AMS, Boston, 1972, pp. 216–221.
92. R. J. Keeler and C. L. Frush, "Coherent wideband processing of distributed targets," in *Proc. Int. Geosci. and Remote Sensing Symp. [IGARSS-83]*, San Francisco, IEEE/URSI, 1983, pp. 3.1–3.5.
93. R. G. Strauch, "A modulation waveform for short-dwell-time meteorological doppler radars," *J. Atmos. Oceanic Technol.*, vol. 5, pp. 512–520, 1988.
94. R. J. Keeler and C. A. Hwang, "Pulse compression for weather radar," in *IEEE Int. Radar Conf.*, Washington, DC, 1995, pp. 1–7.

95. A. Mudukutore, V. Chandrasekar, and R.J. Keeler, "Pulse compression for weather radars," *IEEE Trans. on Geosci. Rem. Sens.*, vol. 36, pp. 125–142, 1998.
96. F. O'Hora and J. Keeler, "Comparison of pulse compression & whitening transform signal processing," in *4th European Radar Conf.*, Barcelona, 2006, pp. 109–112.
97. E. A. Robinson, "Predictive decomposition of time series with application to seismic exploration," *Geophysics*, vol. 32, pp. 418–484, 1967.
98. R. J. Keeler and L. J. Griffiths, "Acoustic doppler extraction by adaptive linear prediction filtering," *J. Acoust. Soc. Amer.*, vol. 61, pp. 1218–1227, 1977.
99. A. C. Koivunen and A. B. Kostinski, "Feasibility of data whitening to improve performance of weather radar," *J. Appl. Meteorol.,* vol. 38, pp. 741–749, 1999.
100. S. M. Torres and D. S. Zrnic, "Whitening in range to improve weather radar spectral moment estimates. Part 1: formulation and simulation," *J. Atmos. Oceanic Technol.*, vol. 20, pp. 1433–1448, 2003.
101. T. Y. Yu, G. Zhang, A. B. Chalamalasetti, R. J. Doviak, and D. S. Zrnic, "Resolution enhancement technique using range oversampling," *J. Atmos. Ocean. Technol*., vol. 23, pp. 228–240, 2006.
102. A. V. Oppenheim and R. W. Schaefer, *Discrete Time Signal Processing*, Englewood Cliffs, NJ: Prentice-Hall, 1989.
103. J. P. Burg, "The relationship between maximum entropy spectra and maximum likelihood spectra," Geophysics, vol. 37, pp. 375–376, 1972.
104. J. Capon, "High resolution frequency-wavenumber spectrum analysis," *Proc. IEEE*, vol. 57, pp. 1408–1419, 1969.
105. S. M. Kay, *Modern Spectral Estimation: Theory and Application,* New York: Prentice-Hall, 1988.
106. S. D. Campbell and S. H. Olson, "Recognizing low-altitude wind shear hazards from doppler weather radar: an artificial intelligence approach," *J. Atmos. Ocean. Technol.*, vol. 4, p. 5–18, 1987.
107. A. L. Pazmany, J. B. Mead, S. M. Sekelsky, and D. J. McLaughlin, "Multi-frequency radar estimation of cloud and precipitation properties using an artificial neural network," in *30th Int. Conf. on Radar Meteorol.*, Munich, AMS, pp. 154–156, 2001.
108. D. Atlas, "Advances in radar meteorology," in *Advances in Geophysics*, Vol. 10, New York: Academic Press, 1964.
109. R. Gunn and G. D. Kinzer, "The terminal velocity of fall for water droplets in stagnant Air," *J. Meteorol.*, vol. 6, pp. 243–248, 1949.
110. J. S. Marshall and W. M. K. Palmer, "The distribution of raindrops with size," *J. Meteorol.*, vol. 4, pp. 186–192, 1948.
111. D. C. Blanchard, "Raindrop size distribution in Hawaiian rains," *J. Meteorol.*, vol. 10, pp. 457–473, 1953.
112. D. M. A. Jones, "3 cm and 10 cm wavelength radiation backscatter from rain," in *5th Weather Radar Conf.*, AMS, Boston, 1955, pp. 281–285.
113. K. L. S. Gunn and J. S. Marshall, "The distribution with size of aggregate snowflakes," *J. Meteorol.*, vol. 15, pp. 452–466, 1958.
114. J. W. Wilson and E. A. Brandes, "Radar measurement of rainfall—a summary," *Bull. Am. Meteorol. Soc.*, vol. 60, pp. 1048–1058, 1979.
115. I. Zawadzki, "On radar-raingage comparison," *J. Appl. Meteorol.*, vol. 14, pp. 1430–1436, 1975.
116. I. Zawadzki, "Factors affecting the precision of radar measurements of rain," in *22cd Conf. Radar Meteorol.*, AMS, Boston, 1984, pp. 251–256.
117. J. Joss. and R. Lee, "Application of radar-gauge comparison to operation precipitation profile corrections," *J. Appl. Meteorol.*, vol. 34, pp. 2612–2630, 1995.
118. U. Germann and J. Joss, "Mesobeta profiles to extrapolate radar precipitation measurements above the Alps to ground level," *J. Appl. Meteorol.*, vol. 41, pp. 542–547, 2002.
119. B. Vignal, G. Galli, J. Joss, and U. Germann, "Three methods to determine profiles of reflectivity from volumetric radar data to correct precipitation estimates," *J. Appl. Meteorol.*, vol. 39, pp. 1715–1726, 2000.

120. F. F. Marzano, E. Picciotti, and G. Vulpiani, "Rain field and reflectivity vertical profile reconstruction from C-band radar volumetric data," *IEEE Trans Geosci Rem. Sens.*, vol. 42, pp. 1033–1046, 2004.
121. J. Bridges and J. Feldman, "An attenuation reflectivity technique to determine the drop size distribution of water clouds and rain," *J. Appl. Meteorol.*, vol. 5, pp. 349–357, 1966.
122. D. S. Zrnic and A. Ryzhkov, "Polarimetry for weather surveillance radars," *Bull. Amer. Meteoro. Soc.*, vol. 80, pp. 389–406, 1999.
123. T. A. Seliga and V. N. Bringi, "Potential use of radar differential reflectivity measurements at orthogonal polarizations for measuring precipitation," *J. Appl. Meteorol.*, vol. 15, pp. 69–76, 1976.
124. M. Sachidananda. and D. S. Zrnic, "Rain Rate estimation from differential polarization measurements," *J. Atmos. Ocean. Tech.*, vol. 4, pp. 588–598, 1987.
125. D. N. Moisseev, C. M. H. Unal, H.W. J. Russchenberg, and L.P. Ligthart, "Improved polarimetric calibration of atmospheric radars," *J. Atmos. Ocean. Tech.*, vol. 19, pp. 1968–1977, 2002.
126. A. Ryzhkov and D. Zrnic, "Assessment of rainfall measurement that uses specific differential phase," *J. Appl. Meteorol.* 35, pp. 2080–2090, 1996.
127. G. Zhang, J. Vivekanandan, and E. Brandes, "A method for estimating rain rate and drop size distribution from polarimetric radar measurements," *IEEE Trans. Geosci. Remote Sens.*, vol. 39**,** pp. 830–841, 2001.
128. J. Vivekanandan, G. Zhang, S.M. Ellis, D. Rajopadhyaya, and S.K. Avery, "Radar reflectivity calibration using differential propagation phase measurement," *Radio Sci.*, vol. 38, pp. 14–1 to 14–14, 2003.
129. P. Kollias, B. A. Albrecht, and F. Marks, Jr., "Why Mie?," *Bull. Amer. Meteor. Soc.*, vol. 83, pp. 1471–1483, 2002.
130. R. J. Doviak, V. Bringi, A. Ryzhkov, A. Zahrai, and D. Zrnic, "Considerations for polarimetric upgrades to the operational WSR-88D radars," *J. Atmos. Ocean. Technol.*, vol. 17, pp. 257–277, 2000.
131. C. Frush, R. J. Doviak, M. Sachidananda, and D. S. Zrnic, "Application of the SZ phase code to mitigate range-velocity ambiguities in weather radars," *J. Atmos. Ocean. Technol.*, vol. 19, pp. 413–430, 2002.
132. J. C. Hubbert, G. Meymaris, and R. J. Keeler, "Range-velocity mitigation via SZ phase coding with experimental S-band radar data," in *31st Conf. on Radar Meteorol.*, AMS, Seattle, 2003 pp. 727–729.
133. M. Sachidananda and D. S. Zrnic, "Clutter filtering and spectral moment estimation for doppler weather radars using staggered pulse repetition time (PRT)," *J. Atmos. Ocean. Technol.*, vol. 17, pp. 323–331, 2000.
134. D. Burgess et al., "Final report on the Joint Doppler Operational Project (JDOP)," 1976–1978, *NOAA Tech. Memo.* ERL NSSL-86, 1979.
135. W. C. Lee and M. M. Bell, "Rapid intensification, eyewall contraction and breakdown of Hurricane Charley (2004) near landfall," *Geophys. Res. Lett.*, vol. 34, L02802, doi:10.1029/2006GL027889, 2007.
136. R. A. Houze Jr., S. S. Chen, W. C. Lee, R. F. Rogers, J. A. Moore, G. J. Stossmeister, J. L. Cetrone, W. Zhao, and M. M. Bell, "The Hurricane Rainband and Intensity Change Experiment (RAINEX): Observations and modeling of Hurricanes Katrina, Ophelia, and Rita (2005)," *Bull. Amer. Meteoro. Soc.*, vol. 87, pp. 1503–1521, 2006.
137. R. J. Donaldson, Jr., "Vortex signature recognition by a doppler radar," *J. Appl. Meteorol.*, vol. 9, pp. 661–670, 1970.
138. J. Wilson and H. P. Roesli, "Use of doppler radar and radar networks in mesoscale analysis and forecasting," *ESA J.*, vol. 9, pp. 125–146, 1985.
139. T. Fujita and F. Caracena, "An analysis of three weather-related aircraft accidents," *Bull. Am. Meteorol. Soc.*, vol. 58, pp. 1164–1181, 1977.
140. T. Fujita, "The downburst," Satellite and Mesometeorology Research Project, Department of the Geophysical Sciences, University of Chicago, 1985.
141. T. Fujita, "The DFW microburst," Satellite and Meteorology Research Project, Department of the Geophysical Sciences, University of Chicago, 1986.

142. J. McCarthy and R. Serafin, "The microburst: hazard to aviation," *Weatherwise*, vol. 37, pp. 120–127, 1984.
143. R. D. Roberts and J. W. Wilson, "A proposed microburst nowcasting procedure using single doppler radar," *J. Appl. Meteorol.,* vol. 28, pp. 285–303, 1989.
144. K. Aydin, T. A. Seliga, and V. Balaji, "Remote sensing of hail with dual linear polarization radar," *J. Clim. Appl. Meteorol.*, vol. 25, pp. 1475–1484, 1986.
145. A. J. Illingworth, J. W. F. Goddard, and S. M. Cherry, "Detection of hail by dual polarization radar," *Nature*, vol. 320, pp. 431–433, 1986.
146. R. M. Lhermitte and D. Atlas, "Precipitation motion by pulse doppler radar," in *9th Weather Radar Conf.*, AMS, Boston, 1961, pp. 218–223.
147. K. A. Browning and R. Wexler, "A determination of kinematic properties of a wind field using doppler radar," *J. Appl. Meteorol*., vol. 7, pp. 105–113, 1968.
148. J. D. Tuttle and G. B. Foote, "Determination of the boundary layer airflow from a single doppler radar," *J. Atmos. Ocean. Technol.*, vol. 7, pp. 218–232, 1990.
149. J. W. Wilson and W. E. Schreiber, "Initiation of convective storms at radar-observed boundary layer convergence lines," *Mon. Weather Rev.*, vol. 114, pp. 2516–2536, 1986.
150. T. W. Weckwerth, C. R. Pettet, F. Fabry, S. J. Park, M. A. LeMone, and J. W. Wilson, "Radar refractivity retrieval: Validation and application to short-term forecasting," *J. Appl. Meteoro.*, vol. 44, pp. 285–300, 2005.
151. M. Hall (ed.), "Special papers: Multiple parameter radar measurements of precipitation," *Radio Sci.*, vol. 19, 1984.
152. R. M. Lhermitte, "Dual-doppler radar observations of convective storm circulations," in *14th Conf. Radar Meteorol.*, AMS, Boston, 1970, pp. 139–144.
153. D. J. McLaughlin, V. Chandrasekar, K. Droegemeier, S. Frasier, J. Kurose, F. Junyent, B. Philips, S. Cruz-Pol, and J. Colom, "Distributed Collaborative Adaptive Sensing (DCAS) for improved detection, understanding and prediction of atmospheric hazards," presented at *85th AMS Annual Meeting*, San Diego, AMS, 2005.
154. F. Junyent, V. Chandrasekar, D. Brunkow, P. C. Kennedy, and D. J. McLaughlin, "Validation of first generation CASA radars with CSU-CHILL," presented at *32cd Conf. Radar Meteorol.*, P10R4, AMS, Albuquerque, 2006.
155. R. E. Carbone, M. Carpenter, and C. Burghart, "Doppler radar sampling limitations in convective storms," *J. Atmos. Ocean. Technol.*, vol. 2, pp. 358–361, 1985.
156. M. Brook and P. Krehbiel, "A fast-scanning meteorological radar," in *16th Conf. Radar Meteorol.*, AMS, Boston, 1975, pp. 26–31.
157. R. J. Keeler and C. L. Frush, "Rapid-scan doppler radar development considerations, Part II: technology assessment," in *21st Conf. Radar Meteorol.* AMS, Boston, 1983, pp. 284–290.
158. P. L. Smith, "Applications of radar to meteorological operations and research," *IEEE Proc.*, vol. 62, pp. 724–725, 1974.
159. C. L. Holloway and R. J. Keeler, "Rapid scan doppler radar: the antenna issues," in *26th Conf. on Radar Meteorol.*, AMS, Norman, 1993, pp. 393–395.
160. L. Josefsson, "Phased array antenna technology for weather radar applications," in *25th Conf. on Radar Meteorol.*, AMS, Paris, 1991, pp. 752–755.
161. R. J. Keeler, "Weather radars of the 21st century: a technology perspective," in *28th Conf. on Radar Meteorol.*, Austin, AMS, 1997, pp. 309–310.
162. P. Meischner, C. Collier, A. Illingworth, J. Joss, and W. Randeu, "Advanced weather radar systems in Europe: The COST-75 action," *Bull. Amer. Meteoro. Soc.*, vol. 78, pp. 1411–1430, 1997.
163. E. Brookner (ed.), *Practical Phased Array Antenna Systems,* Norwich, MA: Artech House, 1991.
164. J. Wurman and M. Randall, "An inexpensive, mobile, rapid scan radar," in *30th Int. Conf. on Radar Meteorol.*, Munich, AMS, 2001, pp. 98–100.
165. J. W. Rogers, L. Buckler, A. C. Harris, M. Keehan, and C. J. Tidwell, "History of the Terminal Area Surveillance System (TASS)," in *28th Conf. Radar Meterol.,* AMS, Austin, 1997, pp. 157–158.

166. W. Benner, W. G. Torok, N. Gordner-Kalani, M. Batista-Carver, and T. Lee, "MPAR program overview and status," presented at *23rd Int. Conf. on Interact. Info. Proc. Sys. (IIPS)*, AMS, San Antonio, 2007.

167. T. Maese, J. Melody, S. Katz, M. Olster, W. Sabin, A. Freedman, and H. Owen, "Dual-use shipborne phased array radar technology and tactical environmental sensing," in *Proc. IEEE National Radar Conf.*, Atlanta, 2001, pp. 7–12.

168. D. E. Forsyth, K. J. Kimpel, D. S. Zrnic, S. Sandgathe, R. Ferek, J. F. Heimmer, T. McNellis, J. E. Crain, A. M. Shapiro, J. D. Belville, and W. Benner, "The national weather radar testbed (phased array)," presented at *18th Int. Conf. on Interact. Info. Proc. Sys. (IIPS)*, AMS, Orlando, 2002.

169. R. L. Trotter, "Design considerations for the NOAA airborne meteorological radar and data system," in *18th Conf. on Radar Meteorol.*, AMS, Atlanta, 1978, pp. 405–408.

170. H. B. Bluestein and R. M. Wakimoto, "Mobile radar observation of severe convective storms," Chapter 5 in *Radar in Atmospheric Science: A collection of essays in honor of David Atlas*, R. Wakimoto and R. Srivastava (eds.), Meteorological Monograph, Vol. 30, Boston: AMS, 2003, pp. 105–136.

171. P. H. Hildebrand, C. A. Walther, C. L. Frush, J. Testud, and F. Baudin, "The ELDORA/ASTRAIA airborne doppler weather radar: goals, design and first field test," *Proc. IEEE*, vol. 12, pp. 1873–1890, 1994.

172. G. M. Heymsfield et al., "The EDOP radar system on the high altitude NASA ER-2 aircraft," *J. Atmos, Oceanic Technol*., vol. 13, pp. 795–809, 1996.

173. L. Li, G. M. Heymsfield, P. E. Racette, L. Tian, and E. Zenker, "A 94-GHz cloud radar system on a NASA high-altitude ER-2 aircraft," *J. Atmos. Oceanic Technol.*, vol. 21, pp. 1378–1388, 2004.

174. D. P. Jorgensen, T. R. Shepherd, and A. S. Goldstein, "A dual-pulse repetition frequency scheme for mitigating velocity ambiguities of the NOAA P-3 airborne doppler radar," *J. Atmos. Oceanic Technol.*, vol. 17, pp. 585–594, 2000.

175. S. L. Durden, E. Im, F. K. Li, W. Ricketts, A. Tanner, and W. Wilson, "ARMAR: An airborne rain mapping radar," *J. Atmos. Oceanic Technol.*, vol. 11, pp. 727–737, 1994.

176. A. Pazmany, R. McIntosh, R. Kelly, and G. Vali, "An airborne 95 GHz dual-polarized radar for cloud studies," *IEEE Trans. Geosci. Remote Sens*, vol. 32, pp. 731–739, 1994.

177. G. Farquharson, E. Loew, W. C. Lee, and J. Vivekanandan, "A new high-altitude airborne millimeter-wave radar for atmospheric research," presented at *Proc. Int. Geosci. Remote Sens. Symp. [IGARSS 2007]*, IEEE, Barcelona, 2007.

178. M. Wolde and A. Pazmany, "NRC Dual-frequency airborne radar for atmospheric research," presented at *32cd Conf. Radar Meteorol.*, P1R.9, Albuquerque, 2005.

179. T. Kozu et al., "Development of precipitation radar on-board the Tropical Rainfall Measuring Mission (TRMM) satellite," *IEEE Trans. Geosci. Remote Sens.*, vol. 39, pp. 102–116, 2001.

180. E. Im et al., "Second-generation precipitation radar (PR-2)," Final Rep. JPL D-22997, NASA Earth Science Instrument Incubator Program, JPL, Calif. Inst. Tech., Pasadena, CA, 2002.

181. R. Meneghini and D. Atlas, "Simultaneous ocean cross-section and rainfall measurements from space with a nadir-looking radar," *J. Atmos. Ocean. Technol.*, vol. 3, pp. 400–413, 1986.

182. L. Liang and R. Meneghini, "A study of air/space-borne dual-wavelength radar for estimation of rain profiles," *Advances in Atmos. Sci,* vol. 22, pp. 841–851, 2005.

183. G. L. Stephens, D. G. Vane, R. J. Boain, G. G. Mace, K. Sassen, Z. Wang, A. J. Illingworth, E. J. O'Connor, W. B. Rossow, S. L. Durden, S. D. Miller, R. T. Austin, A. Benedetti, C. Mitrescu, and the CloudSat Science Team, "The CloudSat mission and the A-train: a new dimension of space-based observations of clouds and precipitation," *Bull. Am. Meteorol. Soc.*, vol. 83, pp. 1771–1790, 2002.

184. E. E. Gossard and R. G. Strauch, *Radar Observations of Clear Air and Clouds*, Amsterdam: Elsevier, 1983.

185. S. Kato T. Tsuda, M. Yamamato, T. Sato, and S. Fukao, "First results obtained with a middle and upper atmosphere (MU) radar," *J. Atmos. Terr. Phys.*, vol. 48, pp. 1259–1267, 1986.

186. S. G. Benjamin, B. E. Schwartz, E. J. Szoke, and S. E. Koch, "The value of wind profiler data in U.S. weather forecasting," *Bull. Amer. Meteor. Soc.*, vol. 85, pp. 1871–1886, 2004.

187. R. E. Carbone, R. Strauch, and G. M. Heymsfield, "Simulation of wind profilers in distributed conditions," in *23rd Conf. Radar Meteorol.*, vol. I, AMS, Boston, 1986, pp. 44–47.

188. R. G. Strauch, B. L. Weber, A. S. Frisch, C. G. Little, D. A. Merritt, K. P. Moran, and D. C. Welsh, "The precision and relative accuracy of profiler wind measurements," *J. Atmos. Ocean. Technol.*, vol. 4, pp. 563–571, 1987.

189. *Proceedings of International Symposia on Tropospheric Profiling*, 1998–present.

190. R. J. Doviak, R. J. Lataitis, and C. L. Holloway, "Cross correlations and cross spectra for spaced antenna wind profilers," *Radio Sci.*, vol. 31, pp. 157–180, 1996.

191. J. S. Van Baelen and A. D. Richmond, "Radar interferometry technique: Three-dimensional wind measurement theory," *Radio Sci.,* vol. 26, pp. 1209–1218, 1991.

192. G. Zhang and R. J. Doviak, "Spaced-antenna interferometry to measure crossbeam wind, shear and turbulence: Theory and formulation," *J. Atmos. Ocean. Technol.*, vol. 24, pp. 791–805, 2007.